pre-print (second revision - post peer review)
Pre-print submitted to Extremes

Environmental contours as Voronoi cells

Andreas Hafver · Christian Agrell · Erik Vanem

Abstract Environmental contours are widely used as basis for design of structures exposed to environmental loads. The basic idea of the method is to decouple the environmental description from the structural response. This is done by establishing an envelope of joint extreme values representing critical environmental conditions, such that any structure tolerating loads on this envelope will have a failure probability smaller than a prescribed value.

Specifically, given an n-dimensional random variable $\mathbf{X}$ and a target probability of failure p_e, an *environmental contour* is the boundary of a set $\mathcal{B} \subset \mathbb{R}^n$ with the following property: For any *failure set* $\mathcal{F} \subset \mathbb{R}^n$, if $\mathcal{F}$ does not intersect the interior of $\mathcal{B}$, then the probability of failure, $P(\mathbf{X} \in \mathcal{F})$, is bounded above by p_e. We work under the assumption that failure sets are convex, which is relevant for many real-world applications.

In this paper, we show that such environmental contours may be regarded as boundaries of Voronoi cells. This geometric interpretation leads to new theoretical insights and suggests a simple novel construction algorithm that guarantees the desired probabilistic properties. The method is illustrated with examples in two and three dimensions, but the results extend to environmental contours in arbitrary dimensions. Inspired by the Voronoi-Delaunay duality in the numerical discrete scenario, we are also able to derive an analytical representation where the environmental contour is considered as a differentiable manifold, and a criterion for its existence is established.

Keywords Multivariate extremes · Convexity · Computational geometry · Differential geometry

1 Introduction and background

1.1 Environmental contours for multivariate extremes analysis

Extreme value analysis typically involves estimating probabilities of rare events or conversely, the values of random variables associated with small probabilities of being exceeded, i.e. high return values associated with long return periods. In the univariate case, such return values are often estimated by quantiles associated with a certain probability of being exceeded. Typically, return periods are long compared to the amount of data that are available, and there is a need to extrapolate beyond the support of the data. Two commonly used approaches for univariate extreme value analysis are the so-called block maxima approach and the peak over threshold approach,

Andreas Hafver
DNV Group Research and Development
E-mail: andreas.hafver@dnv.com

Christian Agrell
Department of Mathematics, University of Oslo, Norway
E-mail: chrisagr@math.uio.no
DNV Group Research and Development
E-mail: christian.agrell@dnv.com

Erik Vanem
Department of Mathematics, University of Oslo, Norway
E-mail: erikvan@math.uio.no
DNV Group Research and Development
E-mail: erik.vanem@dnv.com

where specific probability distributions are known to asymptotically describe the tails of the underlying distributions well, under certain conditions; the generalized extreme value distribution for block maxima and the generalized Pareto distribution for peaks over threshold (see e.g. [14]).

In a multivariate, setting, the notions of return period and return values are ambiguous. There are various definitions of a multivariate extreme, as discussed in [65,22,72,74], giving rise to different versions of multivariate quantiles [13]. The following discussion considers the bivariate case for simplicity, but may easily be generalized to higher dimensions. Typically, a bivariate quantile will be vector-valued and can be expressed on the following form [13]:

$$Q_{X,Y}(p,\varepsilon) = \left\{(x,y) \in \mathbb{R}^2 : F_\varepsilon(x,y) = p\right\},$$

where $F_\varepsilon(x,y)$ correspond to some exceedance or non-exceedance event. Different types of exceedance events give rise to different type of multivariate quantiles and hence different meanings of a multivariate extreme.

Moreover, even with a specific definition of a bivariate extreme, corresponding to a specific choice of $F_\varepsilon(x,y)$, there will not be a unique solution to the extreme quantile problem. Given a pair (x,y) that satisfies the definition of the extreme quantile, one may increase x slightly and reduce y in such a way that the condition is still fulfilled [62]. Hence, there is a continuum of solutions to the extreme value problem in the bivariate, and more generally in the multivariate, case. Hence, the solution will be a curve or a contour in the variable space associated with a non-exceedance probability defined in some way.

Two commonly used examples are the so-called OR and AND events defined in the following ways, where $F_\cdot$ denotes the cumulative distribution function,

$$\begin{aligned} Q^{OR}_{X,Y}(p) &= \left\{(x,y) \in \mathbb{R}^2 : P(X \leq x, Y \leq y) = 1-p\right\} \\ &= \left\{(x,y) \in \mathbb{R}^2 : F_{X,Y}(x,y) = 1-p\right\}, \end{aligned}$$

$$\begin{aligned} Q^{AND}_{X,Y}(p) &= \left\{(x,y) \in \mathbb{R}^2 : P(X \geq x, Y \geq y) = p\right\} \\ &= \left\{(x,y) \in \mathbb{R}^2 : F_X(x) + F_Y(y) - F_{X,Y}(x,y) = 1-p\right\}. \end{aligned}$$

The OR extreme event is defined in terms of simultaneous non-exceedance of the multivariate variables, whereas the AND extreme event is defined in terms of simultaneous exceedance [16]. These definitions correspond to different quantile regions, and different applications would be in favour of using different definitions. Environmental contours represent yet other definitions of multivariate extremes, and there exist different types of contours. Typically, environmental contours are defined in terms of the probability of exceeding a hyperplane, in either physical variable space or a transformed standard normal space, and correspond to marginal exceedances in different directions. Hence, an extreme event along direction θ can be defined as

$$Q^{EC1}_{X,Y}(p;\theta) = \left\{(x,y) \in \mathbb{R}^2 : P\left(X\cos(\theta) + Y\sin(\theta) \geq x\cos(\theta) + y\sin(\theta)\right) = p\right\}, \tag{1}$$

for $\theta \in [0, 2\pi]$.

Other definition of environmental contours, proposed in e.g. [25,12], correspond to multidimensional quantile regions associated with total exceedance probabilities [20,7], see e.g. the discussion in [47].

Some different definitions of bivariate extremes are illustrated in Figure 1 (reproduced from [76]), where the probability of being in the shaded areas correspond to the exceedance probability p. The two first plots correspond to OR and AND extreme events, respectively, the third plot corresponds to environmental contours based on exceedance hyperplanes and the final plot corresponds to the overly conservative definitions in terms of total exceedance probabilities.

In this paper, environmental contours defined in terms of the probabilities of exceeding hyperplanes in physical space will be considered. It is noted that such contours will yield conservative results in structural design if the failure region of a structure is convex. Other contours defined in terms of total exceedance probabilities will always be conservative, for any failure region, but will then be overly conservative if the failure region is indeed convex. For most physical systems, assuming convex failure regions is reasonable, see e.g. some examples in [70].

Environmental contours are often used in probabilistic structural reliability applications, where structural failure may occur in extreme environmental conditions. Hence, the interest is in identifying extreme environmental conditions associated with a small probability of occurrence. A

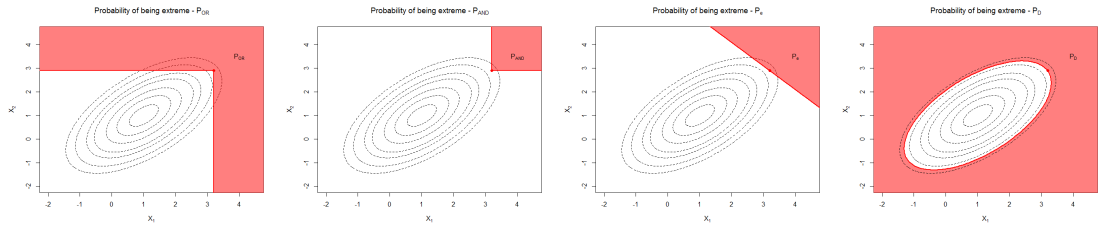

Fig. 1: Different definitions of bivariate extremes

performance function, g is often defined in terms of a set of environmental stochastic input variables, $\mathbf{X} = (X_1, X_2, \ldots, X_p)^T$, so that the structure is deemed safe if $g(\mathbf{X}) > 0$ and will fail if $g(\mathbf{X}) < 0$. $g(\mathbf{X}) = 0$ defines the so-called limit state function and is the boundary between the safe and unsafe regions of the input space. If the environmental variables have joint density function $f_{\mathbf{X}}(\mathbf{x})$, then the reliability R and the probability of failure P_f of the structure can be calculated from

$$R = 1 - P_f = P\left[g(\mathbf{X}) > 0\right] = \int_{g(\mathbf{X})>0} f_{\mathbf{X}}(\mathbf{x}) d\mathbf{x}.$$

These integrals will typically be difficult to solve, and both the joint probability density function $f_{\mathbf{X}}(\mathbf{x})$ and the performance function $g(\mathbf{X})$ can be complicated functions. One common approximate method to solve this problem, is the first order reliability (FORM) method, where the failure boundary at the design point is approximated by a first-order Taylor expansion, see e.g. [29,35] for more details. Typically, it will be assumed that such a linearisation introduces some conservatism, since most structures are likely to have convex failure regions.

With environmental contours, one essentially addresses the inverse problem. Rather than computing the failure probability of a given structure, one assumes that the failure probability is given and then explores what restrictions this poses on possible designs. Environmental contours are typically used in long-term extreme response assessment, and the underlying assumption is that extreme environmental loads and structural responses occur in extreme environmental conditions described by the environmental contours. That is, if the structure can be found to survive all environmental conditions along the environmental contours for a specified exceedance probability, it can be deemed safe according to associated reliability targets. In this way, computationally expensive response analyses may only be carried out for a limited set of environmental conditions in order to perform long-term extreme response analyses. Environmental contours also effectively de-couples the environmental descriptions from the structural problem, and once established, a set of environmental contours may be applied to a range of different structural designs. Environmental contours are hence not a function of the performance function of the structure (which is often unknown and can only be calculated for particular input by computationally heavy calculations), but only relies on the joint distribution of the environmental input variables. This latter is typically established based on fitting parametric distributions to data of the environmental variables, for example using the conditional modelling approach [11,31] using copulas [79,69], the conditional extremes model [30,67], or any other modelling approach [38]. In this context, statistical distributions that accurately captures the tail behaviour of multivariate environmental data are very relevant, for example based on multivariate extensions of extreme value theories such as the Pickands-Balkema-de Haan theorem, see e.g. [40,15,61].

Considering the various definitions of extremes, as illustrated in Figure 1, which one is most appropriate will depend on the application (i.e. the shape of the limit state function), and the shaded areas in the plots should best correspond to the failure region. It can be seen that the extremes defined in terms of exceedance hyperplanes correspond to a linearisation of the failure surface, and is in line with the rationale behind the FORM approximation. For convex failure sets, this will represent a conservative estimate of the failure probability.

1.2 A brief review of environmental contours

The use of environmental contours is a well-established practice in design of marine structures, and helps the designer to identify design sea states corresponding to extreme environmental loads asso-

ciated with a certain return period. The concept of environmental contours is an efficient method for estimating multivariate extreme conditions, and it is an alternative to full long-term response analysis in situations where this is not feasible. An environmental contour is a set constructed based on a joint probability distribution for the relevant input parameters, for example significant wave height and wave period. The environmental contour method is advised in standards and recommended practices such as [23,57].

The concept of environmental contours was first introduced by [26,27] as a means to study the joint distribution of significant wave height and wave period of ocean waves. These early environmental contours were based on constant densities, but the concept of environmental contours was developed further by [80] by using the Inverse First Order Reliability Method (IFORM) and considering exceedance probabilities in the transformed standard normal space [29]. The IFORM method avoids unnecessary conservatism in the equi-density contours [41], and has since then become the most applied contour method. Several applications of the environmental contour method in marine engineering and design are reported in the literature [56,81,5,64,6,3,4,39,28,54]. A comparison study presented in [1] investigated the influence of the choice of contour method on some vessel responses.

Environmental contours continues to be an active area of research, and several modified approaches have been suggested in recent years, e.g., a dynamical IFORM method [45], a modified approach to account for non-monotonic behaviour of the responses [43], an approach including pre-processing and principal component analysis prior to estimate IFORM contours [19], contours for sub-populations such as directional sectors or seasonality [72,33], contours for a combination of circular and linear variables [24], contours for copula-based joint distributions [68,51] and contours based on a direct IFORM approach [18]. Contours for buffered failure probabilities were proposed in [17] and contours based on a particular version of the inverse second order reliability method (ISORM) were derived in [12]. Recently, the initial equi-density method was revisited in [25]. The uncertainties associated with environmental contours due to uncertainties in the underlying joint distribution model and due to sampling variability are investigated in [53] and [77], respectively, and weighted environmental contours based on combining data from different datasets were explored in [73]. Reviews of various contour methods are presented in e.g. [48,62].

An alternative approach to constructing environmental contours that avoids the transformation into standard normal space, but rather defines exceedance probabilities in the original parameter space, was proposed in [35,37]. This is based on Monte Carlo simulations from the joint distribution of environmental parameters. Initial inaccuracies due to insufficient number of Monte Carlo samples were overcome by a scheme for tail sampling as outlined in [36]. It is argued that the contours obtained in this way have more well defined probabilistic properties. An evaluation of the properties of the IFORM-based environmental contours is presented in [34]. However, in some situations it is found that the direct sampling contours may contain irregularities in the form of small loops, as discussed in [37]. One reason for this is related to the Monte Carlo variance and the fact that the contours are estimated with respect to a finite sample from the joint distribution, and the issue may be resolved by increasing the number of Monte Carlo samples. However, the reason may also be genuine features of the underlying joint distribution, i.e. that the joint distribution does not admit a proper convex environmental contour. An illustrative example is given in [37], which shows a scenario where it is not possible to obtain an environmental contour with the property that the exceedance probability for each supporting hyperplane is constant. We reproduce this example herein, in Figure 4.

A comparison study on the IFORM and the Monte Carlo-based approach to environmental contours was presented in [75], which demonstrated that in certain cases, notably different contours are obtained. The comparison study was extended to consider various simple structural problems in [70] and to compare contour-based methods to response-based methods in [78].

Even though many structural problems depend on more than two environmental variables, most applications of environmental contours are restricted to two-dimensional contours. For example, in the multivariate problem addressed in [55], environmental contours were only calculated for pairs of variables. However, some examples of three-dimensional contours based on the IFORM approach, are shown in [44,63,59,52]. An extension of the direct sampling approach to three-dimensional problems was outlined in [71], and this method was applied to the tension in a mooring line of a semi-submersible in [60]. However, even though extensions of the direct sampling approach to environmental contour to higher dimensional problems is indeed possible, calculating the contours becomes increasingly cumbersome in higher dimensions.

1.3 Contribution of this paper

In this paper, an alternative way of constructing environmental contours is proposed, that easily generalises to arbitrary dimensions. With this method, environmental contours can be described as boundaries of Voronoi cells, which may easily be found from standard software packages at reasonable computational costs. The method makes use of Monte Carlo samples from the underlying distribution, but overcomes the common loop-problem of direct sampling methods, and can be used to produce convex contours with the desired probabilistic properties.

In Section 2 we briefly review the mathematical definition of environmental contours. In Section 3 we give a general introduction to Voronoi cells, before showing in Section 4 that environmental contours may be interpreted as boundaries of Voronoi cells. In Section 5 we generalise results from Section 4 to the continuous limit, deriving additional theoretical insights, including an analytic formula for environmental contours in terms of a given percentile function. Section 6 details the practical application of the proposed algorithm, and examples in two and three dimensions are provided in Section 7. Some concluding remarks are provided in section 8. For brevity, proofs are contained in appendices.

2 Definition of environmental contours

We consider a structure or component exposed to some environmental loads. The environmental loads can be represented by a vector of variables $\mathbf{X} \in \mathcal{X} \subseteq \mathbb{R}^n$, distributed according to some multivariate probability distribution $f_{\mathbf{X}}(\mathbf{x})$. We further define a performance function $g(\mathbf{x})$, where $\mathbf{x}$ is a specific environmental state, such that the structure or component remains intact/functioning as long as $g(\mathbf{x}) \geq 0$, and fails if $g(\mathbf{x}) < 0$.

The failure region $\mathcal{F} = \{\mathbf{x} \in \mathcal{X} : g(\mathbf{x}) < 0\}$ and the corresponding failure probability $p_f = P(\mathbf{X} \in \mathcal{F}) = \int_{\mathcal{F}} f_{\mathbf{X}}(\mathbf{x})d\mathbf{x}$ are generally unknown. However, in many cases, one may argue based on physics that $\mathcal{F}$ must be convex. Therefore, in such situations, if we can find another convex set $\mathcal{B}$ such that $g(\mathbf{x}) \geq 0 \ \forall \mathbf{x} \in \mathcal{B}$, it follows from convexity theory that there exist a *supporting hyperplane* Π that separates $\mathcal{B}$ and $\mathcal{F}$ (i.e. $\mathcal{B} \subseteq \Pi^-$ and $\mathcal{F} \subseteq \Pi^+$, where Π^- and Π^+ are the two half spaces separated by Π), and $p_f \leq P(\mathbf{X} \in \Pi^+) = \int_{\Pi^+} f_{\mathbf{X}}(\mathbf{x})d\mathbf{x}$.

We may construct the set

$$\mathcal{B}_{p_e} = \bigcap_{\mathbf{u} \in \mathcal{U}} \Pi^-_{p_e}(\mathbf{u}), \tag{2}$$

where $\mathcal{U}$ denotes the set of all unit vectors in $\mathbb{R}^n$, i.e.

$$\mathcal{U} = \{\mathbf{u} \in \mathbb{R}^n \mid \|\mathbf{u}\| = 1\},$$

and $\Pi^-_{p_e}(\mathbf{u})$ is the half-space normal to $\mathbf{u}$ with the property that $P(\mathbf{X} \in \Pi^-_{p_e}(\mathbf{u})) = 1 - p_e$. More precisely,

$$\Pi^-_{p_e}(\mathbf{u}) = \{\mathbf{x} : \mathbf{u} \cdot \mathbf{x} \leq C_{p_e}(\mathbf{u})\}, \tag{3}$$

where C_{p_e} denotes the p_e-level percentile function, defined by

$$C_{p_e}(\mathbf{u}) = \inf\{c : P(\mathbf{u} \cdot \mathbf{X} > c) \leq p_e\}. \tag{4}$$

We will assume that the distribution of $\mathbf{X}$ is absolutely continuous with respect to the Lebesgue measure on $\mathbb{R}^n$, so the function $C_{p_e}(\mathbf{u})$ in (4) is well defined. We note also that (2) uniquely defines a convex set, as all half-spaces $\Pi^-_{p_e}(\mathbf{u})$ are convex.

Depending on the distribution of $\mathbf{X}$, the definition of $\mathcal{B}_{p_e}$ in (2) does not imply that all hyperplanes $\Pi_{p_e}(\mathbf{u})$ intersect $\mathcal{B}_{p_e}$. (See for instance the discussion in Section 4 or the example given in Figure 8.) In the case where all hyperplanes $\Pi_{p_e}(\mathbf{u})$ intersect $\mathcal{B}_{p_e}$, the authors in [37] state that $\mathbf{X}$ *admits* a p_e-contour. We will make use of the equivalent definition below.

Definition 1 Let $\mathcal{B}_{p_e}$ be a nonempty convex set in $\mathbb{R}^n$ and $p_e \in (0, 0.5)$. If

$$P(\mathbf{X} \in \Pi^+) \leq p_e$$

for any supporting half-space Π^+ of $\mathcal{B}_{p_e}$, we say that $\partial\mathcal{B}_{p_e}$ is a valid environmental contour of $\mathbf{X}$ with respect to the target probability p_e. If (1) holds with equality for all the supporting half-spaces Π^+, then $\partial\mathcal{B}_{p_e}$ is also a proper environmental contour.

In the case where a proper convex environmental contour exists, it is necessarily given by the representation in (2). This follows from the fact that any closed convex subset $\mathcal{B} \subset \mathbb{R}^n$ is the intersection of all supporting half-spaces that contain $\mathcal{B}$ (see e.g. Theorem 3.6.18 in [42]). If all those half-spaces satisfy (1) with equality, then the representation in (2) follows. For reference we state this in a separate proposition.

Proposition 1 *Assume that the random variable* $\mathbf{X}$ *admits a proper convex environmental contour* $\partial\mathcal{B}_{p_e}$ *with respect to a target probability* $p_e \in (0, 0.5)$. *Then the closure of* $\mathcal{B}_{p_e}$ *is uniquely defined by* (2).

In the following we will start by assuming that $\mathbf{X}$ admits a proper convex environmental contour, and also that the probabilities $P(\mathbf{X} \in \Pi^+)$ can be computed without error. After introducing the connection with Voronoi cells and an algorithm for constructing $\mathcal{B}_{p_e}$, we present an approach that can be used when these assumptions are relaxed.

3 Voronoi cells

The Voronoi diagram is a fundamental data structure in computational geometry that has found applications in a variety of fields, including physics, biology, cartography, crystallography, ecology, geology, anthropology, and meteorology to mention some [58]. Given a set of points $p_1, \dots p_k$ in a metric space $\mathcal{X}$, the Voronoi diagram is defined as the partitioning of $\mathcal{X}$ into regions $R_1, \dots R_k$, such that R_i consists of all points in $\mathcal{X}$ whose distance to p_i is not greater than their distance to any other p_j for $j \neq i$. The region R_i is often referred to as the *Voronoi cell* of p_i (with respect to the remaining points p_j, $j \neq i$).

In its canonical form, a Voronoi diagram is constructed from a set of points in $\mathbb{R}^n$ endowed with the Euclidean metric, and other alternatives are usually referred to as *Generalised Voronoi diagrams* [46,2]. In this paper, we will consider the Voronoi cell of a point $\mathbf{o} \in \mathbb{R}^n$ with respect to a set $S \subset \mathbb{R}^n$. We denote the Voronoi cell by $\mathrm{Vor}(\mathbf{o}, S)$. This consists of the set of points that are at least as close to $\mathbf{o}$ as any point in S, measured by the Euclidean distance in $\mathbb{R}^n$, i.e.

$$\mathrm{Vor}(\mathbf{o}, S) = \left\{ \mathbf{x} \in \mathbb{R}^n \mid \|\mathbf{x} - \mathbf{o}\| \leq \inf_{\mathbf{s} \in S} \|\mathbf{x} - \mathbf{s}\| \right\}. \tag{5}$$

To motivate the algorithm presented in this paper we will make use of the rather trivial property that if the set S is finite, then it is equivalent to the definition of point Voronoi cells as illustrated in Figure 2. In the following section we show that an environmental contour can be represented as a Voronoi cell of the form (5). A numerical approximation is then achieved by replacing the set S in (5) with a finite subset, where available algorithms developed for canonical (point) Voronoi diagrams can be used. In this case we will also make use of the Delaunay triangulation of the finite point set, that correspond to the dual graph of the Voronoi diagram. This is illustrated for points in the plane in Figure 2, and we refer to [58] for further details.

4 Environmental contours as boundaries of Voronoi cells

In this section we give a representation of the environmental contours described in Section 2 using Voronoi cells of the form (5). We start by introducing the general construction and present some theoretical properties, in anticipation of a practical procedure for approximation of environmental contours that will follow in Section 6.

In Section 2 we defined the environmental contours in terms of half-spaces that were parametrized by their perpendicular distance to the origin. However, a half-space may equivalently be parametrized in terms of perpendicular distance to any other point $\mathbf{o} \in \mathbb{R}^n$, i.e.

$$\Pi^-_{p_e}(\mathbf{u}) = \{\mathbf{x} : \mathbf{u} \cdot (\mathbf{x} - \mathbf{o}) \leq C^{\mathbf{o}}_{p_e}(\mathbf{u})\}, \tag{6}$$

with

$$C^{\mathbf{o}}_{p_e}(\mathbf{u}) = \inf\{c : P(\mathbf{u} \cdot (\mathbf{X} - \mathbf{o}) > c) \leq p_e\}. \tag{7}$$

By comparing (2) and (7) it is evident that

$$C^{\mathbf{o}}_{p_e}(\mathbf{u}) = C_{p_e}(\mathbf{u}) - \mathbf{u} \cdot \mathbf{o}, \tag{8}$$

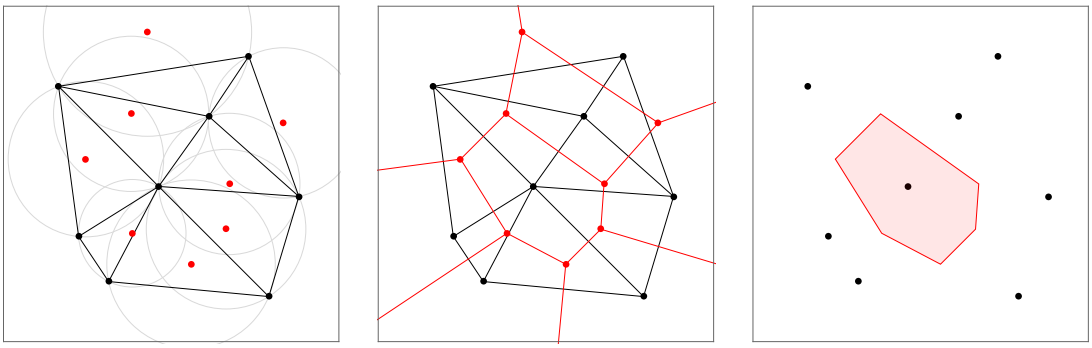

Fig. 2: Illustration of Delaunay triangulation and Voronoi diagram of a set of points. a) A Delaunay triangulation of the 8 **black points** is defined as a triangulation such that no point lies inside the circumcircle of any triangle. The **red points** are the centers of each circumcircle. b) The Voronoi diagram corresponds to the dual graph of the Delaunay triangulation, with the **red circumcenters** of the Delaunay triangles as Voronoi vertices. Two Voronoi vertices are joined by an edge (**red lines**) if the corresponding Delaunay triangles share a face. c) The Voronoi cell of a Voronoi vertex, which correspond to the set of points that are closer to that vertex than to any of the other Voronoi vertices. This generalises to n dimensions, where the Delaunay triangulation corresponds to n-simplices such that no Delaunay vertex lie inside the circum-hypersphere of any n-simplex, and the Voronoi vertices correspond to the centers of circum-hyperspheres, which are joined by edges defined by shared hyperplanes between the Delaunay n-simplices.

and that the two definitions of $\Pi^-_{p_e}(\mathbf{u})$ given in (3) and (6) are equivalent.

Using this alternative parametrization for $\Pi^-_{p_e}(\mathbf{u})$, we define the set $\mathcal{S}^{\mathbf{o}}_{p_e}(U)$ as

$$\mathcal{S}^{\mathbf{o}}_{p_e}(U) = \{\mathbf{s}^{\mathbf{o},\mathbf{u}}_{p_e} = \mathbf{o} + 2C^{\mathbf{o}}_{p_e}(\mathbf{u})\mathbf{u}\}_{\mathbf{u}\in U}, \tag{9}$$

where U is a subset of the unit vectors in $\mathbb{R}^n$.

A point $\mathbf{s}^{\mathbf{o},\mathbf{u}}_{p_e} \in \mathcal{S}^{\mathbf{o}}_{p_e}(U)$ represents the reflection of the point $\mathbf{o} \in \mathbb{R}^n$ with respect to the boundary of the half-space $\Pi^-_{p_e}(\mathbf{u})$ (i.e. with respect to $\Pi_{p_e}(\mathbf{u})$). Stated differently, the half-space $\Pi^-_{p_e}(\mathbf{u})$ contains all points that are closer to $\mathbf{o}$ than to $\mathbf{s}^{\mathbf{o},\mathbf{u}}_{p_e}$. Intuitively, if $\mathbf{o}$ is in the interior of $\mathcal{B}_{p_e}$, then all points in the convex set $\mathcal{B}_{p_e}$ should be closer to $\mathbf{o}$ than to any point in $\mathcal{S}^{\mathbf{o}}_{p_e}(U)$. This means that $\mathcal{B}_{p_e}$ is included in the Voronoi cell of $\mathbf{o}$ with respect to the set of points $\mathcal{S}^{\mathbf{o}}_{p_e}(U)$. The latter insight is stated formally as a lemma below.

Lemma 1 *Let $\mathcal{B}_{p_e}$ be defined as in (2). Then*

$$\mathbf{o} \in \mathcal{B}_{p_e} \iff C^{\mathbf{o}}_{p_e}(\mathbf{u}) \geq 0 \;\forall\; \mathbf{u} \in \mathcal{U},$$
$$\mathbf{o} \in \mathcal{B}_{p_e} \setminus \partial\mathcal{B}_{p_e} \iff C^{\mathbf{o}}_{p_e}(\mathbf{u}) > 0 \;\forall\; \mathbf{u} \in \mathcal{U}.$$

Furthermore, if $\mathbf{o} \in \mathcal{B}_{p_e} \setminus \partial\mathcal{B}_{p_e}$ we have for any subset $U \subseteq \mathcal{U}$ that

$$Vor(\mathbf{o}, \mathcal{S}^{\mathbf{o}}_{p_e}(U)) = \bigcap_{\mathbf{u}\in U} \Pi^-_{p_e}(\mathbf{u}),$$

where $Vor(\cdot,\cdot)$ is the Voronoi cell as defined in (5).

The proof is given in Appendix A. Using this result we arrive at the following proposition that motivates the algorithm presented in this paper.

Proposition 2 *Let $\mathcal{B}_{p_e}$ be defined as in (2), and let U_1 and U_2 be sets of unit vectors in $\mathbb{R}^n$, such that $U_1 \subseteq U_2 \subseteq \mathcal{U}$. If $\mathbf{o} \in \mathcal{B}_{p_e} \setminus \partial\mathcal{B}_{p_e}$ then the following holds:*

$$\mathcal{B}_{p_e} = Vor(\mathbf{o}, \mathcal{S}^{\mathbf{o}}_{p_e}(\mathcal{U})) \subseteq Vor(\mathbf{o}, \mathcal{S}^{\mathbf{o}}_{p_e}(U_2)) \subseteq Vor(\mathbf{o}, \mathcal{S}^{\mathbf{o}}_{p_e}(U_1)).$$

This proposition follows directly from Lemma 1 (see Appendix B for details). The first interesting observation is that the environmental contour, $\partial\mathcal{B}_{p_e}$, can be represented as the boundary of the Voronoi cell $\mathrm{Vor}(\mathbf{o}, \mathcal{S}^{\mathbf{o}}_{p_e}(\mathcal{U}))$. This insight immediately suggests a new algorithm for numerical approximation of environmental contours, by replacing the set of unit vectors $\mathcal{U}$ with a finite subset $U = \{\mathbf{u}_i \mid \mathbf{u}_i \in \mathcal{U}, i = 1, \ldots, k\}$, as illustrated in Figure 3. The proposition also states that

any such approximation of a *proper* convex environmental contour will be conservative, in the sense that the resulting Voronoi cell is guaranteed to contain $\mathcal{B}_{p_e}$. Accordingly, any approximation will be a *valid* convex environmental contour. Moreover, including more unit vectors in the set U improves the approximation (or at least does not make it worse). Intuitively, the error in the approximation can be made arbitrarily small, although this naturally will depend on the sampling strategy used.

A natural procedure for approximating $\mathcal{B}_{p_e}$ could therefore be as follows:

Step 1 Select a set of unit vectors $U = \{\mathbf{u}_j\}_{j=1}^{M}$.
Step 2 Compute $C_{p_e}(\mathbf{u}_1), \ldots, C_{p_e}(\mathbf{u}_M)$.
Step 3 Compute $\mathcal{S}^{\mathbf{o}}_{p_e}(U)$ for some $\mathbf{o} \in \mathcal{B}_{p_e} \setminus \partial\mathcal{B}_{p_e}$.
Step 4 Compute the Voronoi cell of $\mathbf{o}$ with respect to $\mathcal{S}^{\mathbf{o}}_{p_e}(U)$.

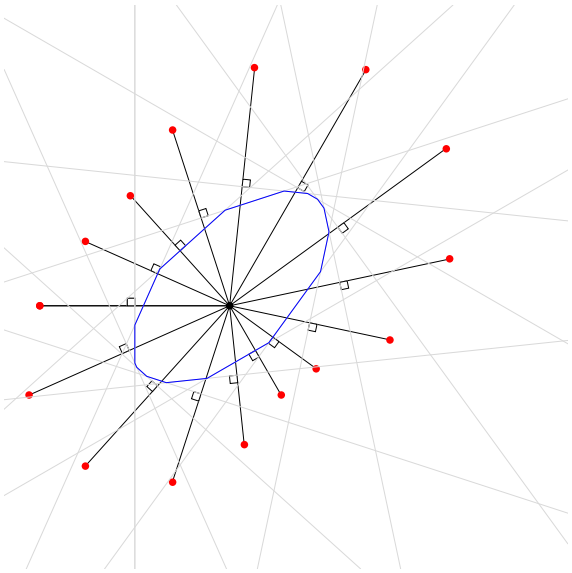

Fig. 3: Construction of environmental contour using the Voronoi method. The black point is the chosen origin $\mathbf{o} \in \mathcal{B}_{p_e} \setminus \partial\mathcal{B}_{p_e}$. The red points correspond to the finite set $\mathcal{S}^{\mathbf{o}}_{p_e}$. The boundaries of the half planes $\Pi^{-}_{p_e}(\mathbf{u})$ half way between $\mathbf{o}$ and the respective points $\mathbf{s}^{\mathbf{o},\mathbf{u}}_{p_e} \in \mathcal{S}^{\mathbf{o}}_{p_e}$ are drawn as light grey lines, and their perpendicularity on the black lines from $\mathbf{o}$ to $\mathbf{s}^{\mathbf{o},\mathbf{u}}_{p_e}$ is indicated with small squares. The boundary of the Voronoi cell of $\mathbf{o}$ with respect to $\mathcal{S}^{\mathbf{o}}_{p_e}$ is drawn in blue, and it can be seen that the grey lines are tangential on the Voronoi cell.

Under the assumption that a proper convex environmental contour exists (for the given random variable $\mathbf{X}$ and target probability p_e), the set $\widehat{\mathcal{B}}_{p_e} = \mathrm{Vor}(\mathbf{o}, \mathcal{S}^{\mathbf{o}}_{p_e}(U))$ is guaranteed to contain $\mathcal{B}_{p_e}$, and the difference can be made arbitrarily small by including sufficiently many unit vectors in U. For practical application, however, it is not reasonable to assume that the function $C_{p_e}(\mathbf{u})$ can be computed exactly, and we might not have *a priori* a point $\mathbf{o} \in \mathcal{B}_{p_e} \setminus \partial\mathcal{B}_{p_e}$. We will postpone these questions to Section 6. For now, we will assume that a point $\mathbf{o} \in \mathcal{B}_{p_e} \setminus \partial\mathcal{B}_{p_e}$ is given and that the function $C_{p_e}(\mathbf{u})$ can be evaluated without error, in order to study the final major assumption. Namely, that the random variable of interest $\mathbf{X}$ admits a proper convex environmental contour for the target probability p_e.

In practice, it might not be possible to determine *a priori* whether a proper convex environmental contour exists. To see how we might account for this issue, we first study what will happen if $\mathbf{X}$ *does not* admit a proper convex environmental contour. In Figure 4 we reproduce the example given in [37], illustrating the scenario where a supporting half-space can have exceedance probability larger than p_e. That is, one of the hyperplanes $\Pi^{-}_{p_e}(\mathbf{u})$ in (2) does not intersect $\mathcal{B}_{p_e}$. Hence, if a scenario such as the one in Figure 4 a) occurs, this means that a proper environmental contour cannot exist (for the selected target probability p_e). As we illustrate in the figure, there is an interesting connection with the dual representation of the Voronoi cell, the Delaunay triangulation, that can be exploited when studying this problem. We recall that every vertex on a Voronoi cell corresponds to the circumcenter of a Delaunay triangle (in general a Delaunay simplex for higher dimensions), and we say that a Delaunay triangulation connects two points $\mathbf{a}, \mathbf{b} \in \mathcal{X}$ if both $\mathbf{a}$ and $\mathbf{b}$ are part of the same triangle (simplex) in the triangulation. With this terminology, we may state the observation made in Figure 4 formally as follows.

Proposition 3 *Assume $\partial\mathcal{B}_{p_e}$ is a proper convex environmental contour with $\mathcal{B}_{p_e}$ defined as in (2). Let $\mathcal{S}^{\mathbf{o}}_{p_e}(U)$ be defined as in (9) for some finite set $U \subset \mathcal{U}$, and $\mathbf{o} \in \mathcal{B}_{p_e} \setminus \partial\mathcal{B}_{p_e}$.*

Then, for all $\mathbf{s} \in \mathcal{S}^{\mathbf{o}}_{p_e}(U)$, there exists a Delaunay triangulation of the point set $\{\mathbf{o}\} \cup \mathcal{S}^{\mathbf{o}}_{p_e}(U)$ that connects $\mathbf{s}$ and $\mathbf{o}$.

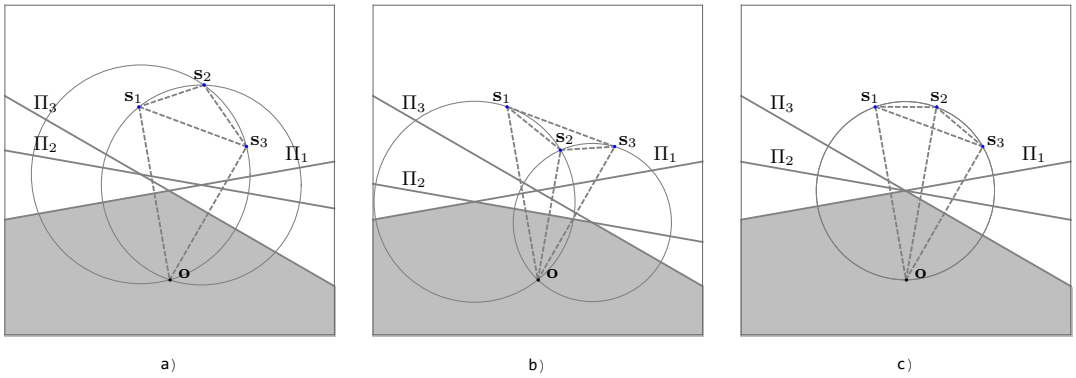

Fig. 4: Three points from $\mathcal{S}^{\mathbf{o}}_{p_e}(U)$ with corresponding hyperplanes, $\mathbf{s}_i = \mathbf{s}^{\mathbf{o},\mathbf{u}_i}_{p_e}$ and $\mathit{\Pi}_i = \mathit{\Pi}_{p_e}(\mathbf{u}_i)$ for three unit vectors $U = \{\mathbf{u}_1, \mathbf{u}_2, \mathbf{u}_3\}$. The Voronoi cell $\text{Vor}(\mathbf{o}, \mathcal{S}^{\mathbf{o}}_{p_e}(U))$ corresponds to the shaded area in each figure, and the dual Delaunay triangulation is indicated with dashed lines. a) $\mathit{\Pi}_2$ is not a supporting hyperplane of $\text{Vor}(\mathbf{o}, \mathcal{S}^{\mathbf{o}}_{p_e}(U))$ since $\mathbf{s}_2$ is not connected to $\mathbf{o}$ by any Delaunay edge. b) All planes $\mathit{\Pi}_i$ intersect $\text{Vor}(\mathbf{o}, \mathcal{S}^{\mathbf{o}}_{p_e}(U))$ as $\mathbf{s}_i$ is connected to $\mathbf{o}$ by a Delaunay edge for all i. c) The Delaunay triangulation is not unique, and $\mathit{\Pi}_2$ only intersects a vertex of $\text{Vor}(\mathbf{o}, \mathcal{S}^{\mathbf{o}}_{p_e}(U))$.

A proof of Proposition 3 is given in Appendix C, where we refer to [58] for results regarding the Voronoi-Delaunay duality. We may also make use of the fact that a Delaunay triangulation of a point set is unique if the points are in *general position*. In the general n-dimensional case, a set $\mathbf{P}$ of points is in *general position* if the affine hull of $\mathbf{P}$ is n-dimensional, and there is no subset of $n+2$ points in $\mathbf{P}$ that lie on the boundary of a ball whose interior does not intersect $\mathbf{P}$. Figure 4 c) shows a scenario where this condition is violated. Here, the affine hull of the set $\mathbf{P} = \{\mathbf{o}, \mathbf{s}_1, \mathbf{s}_2, \mathbf{s}_3\}$ is clearly 2-dimensional, but the four points in $\mathbf{P}$ all lie on a circle (whose interior does not contain any points in $\mathbf{P}$). Hence, the Delaunay triangulation is not unique. There are in fact two possible Delaunay triangulations as illustrated in Figure 4 c), $\{\{\mathbf{o}, \mathbf{s}_1, \mathbf{s}_3\}, \{\mathbf{s}_1, \mathbf{s}_2, \mathbf{s}_3\}\}$ and $\{\{\mathbf{o}, \mathbf{s}_1, \mathbf{s}_2\}, \{\mathbf{o}, \mathbf{s}_2, \mathbf{s}_3\}\}$. Using this condition for uniqueness together with Proposition 3, we immediately achieve the following convenient result.

Corollary 1 *Under the assumptions of Proposition 3, if also the points in* $\{\mathbf{o}\} \cup S^{\mathbf{o}}_{p_e}(U)$ *are in general position, then the Delaunay triangulation is unique and connects all points* $\mathbf{s} \in \mathcal{S}^{\mathbf{o}}_{p_e}(U)$ *with* $\mathbf{o}$.

Corollary 1 gives a criterion for checking whether a proper convex environmental contour exists, and can be used to identify why an environmental contour is not proper convex (i.e., identify the directions $\mathbf{u}$ for which $\mathit{\Pi}_{p_e}(\mathbf{u})$ is not a supporting hyperplane of $\mathcal{B}_{p_e}$). The general idea is also illustrated in Figure 5, where we can conclude that no proper convex environmental contour exists, for the given distribution of $\mathbf{X}$ and target probability p_e, as the grey shaded triangle contains a point $\mathbf{s} \in S^{\mathbf{o}}_{p_e}(U)$ which is not connected with $\mathbf{o}$.

5 Voronoi contours in the continuous limit

Besides constructing environmental contours numerically, it is also of interest to understand more theoretically the connection between probability distributions $f_{\mathbf{X}}(\mathbf{x})$ and corresponding environmental contours $\mathcal{B}_{p_e}$ for some target probability p_e. From a more practical perspective, if the insight we get this way can help us understand the conditions for when a proper environmental contour can be obtained, then that can be very useful. With the results we have obtained so far, and the intuition that comes from viewing environmental contours as Voronoi cells, we get an opportunity to investigate this connection, by considering the geometric relationship between the p_e-level percentile function C_{p_e} and the boundary $\partial\mathcal{B}_{p_e}$.

We can begin by considering the illustrations in Figure 4 and Figure 5, and imagine what happens as more points are added, moving to the limit as $S^{\mathbf{o}}_{p_e}(U) \to S^{\mathbf{o}}_{p_e}(\mathcal{U})$. Consider the Delaunay triangle $\{\mathbf{o}, \mathbf{s}_2, \mathbf{s}_3\}$ in Figure 4 b). This triangle has the property that its circumcircle contains no other points from $S^{\mathbf{o}}_{p_e}(U)$ in its interior. As the points $\mathbf{s}_2$ and $\mathbf{s}_3$ move arbitrarily close together, the

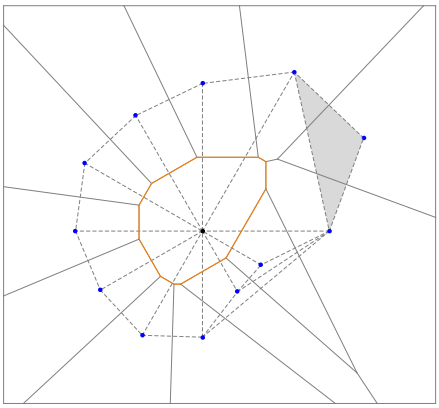

Fig. 5: Illustration of the idea behind Proposition 3 and Corollary 1 in 2D. The dashed lines shows the Delaunay triangulation of the points $\{\mathbf{o}\} \cup S^{\mathbf{o}}_{p_e}(U)$, which are in general position. The grey triangle contains a point $\mathbf{s} \in S^{\mathbf{o}}_{p_e}(U)$ that is not connected to $\mathbf{o}$. Hence, no proper convex environmental contour exists for the selected probability p_e and the random variable $\mathbf{X}$ used to generate $S^{\mathbf{o}}_{p_e}(U)$.

circumcircle of this "triangle" is the circle that contain $\mathbf{o}$ and is tangential to $\mathbf{s}_2 \approx \mathbf{s}_3$. Moreover, the center of this circle is a point on $\partial\mathcal{B}_{p_e}$. From this intuition we arrive at the geometric property of proper convex environmental contours, which is illustrated in Figure 6. We state this formally in Proposition 4, with a proof given in Appendix D.

Proposition 4 *Assume $\partial\mathcal{B}_{p_e}$ is a proper convex environmental contour with $\mathcal{B}_{p_e}$ defined as in (2). Let $\mathcal{S}^{\mathbf{o}}_{p_e}(\mathcal{U})$ be as in (9) and define, for any $\mathbf{b} \in \partial\mathcal{B}_{p_e}$ and $\mathbf{o} \in \mathcal{B}_{p_e} \setminus \partial\mathcal{B}_{p_e}$, the n-dimensional ball $\mathcal{W}^{\mathbf{o}}(\mathbf{b}) = \{\mathbf{x} \in \mathbb{R}^n \mid \|\mathbf{x} - \mathbf{b}\| \leq \|\mathbf{b} - \mathbf{o}\|\}$.*

Then for any $\mathbf{u} \in \mathcal{U}$, there exists some $\mathbf{b} \in \Pi_{p_e}(\mathbf{u}) \cap \partial\mathcal{B}_{p_e}$ such that $\mathcal{S}^{\mathbf{o}}_{p_e}(\mathcal{U}) \cap \mathcal{W}^{\mathbf{o}}(\mathbf{b}) \subseteq \partial\mathcal{W}^{\mathbf{o}}(\mathbf{b})$, and $\mathbf{s}^{\mathbf{o},\mathbf{u}}_{p_e} \in \partial\mathcal{W}^{\mathbf{o}}(\mathbf{b})$.

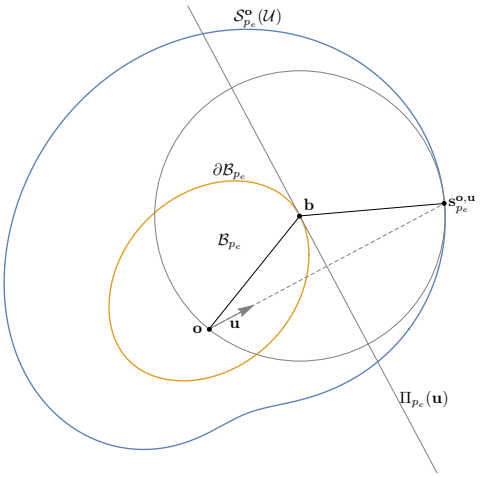

Fig. 6: Geometric illustration of Proposition 4 in 2D. For any $\mathbf{u} \in \mathcal{U}$ there exists some $\mathbf{b} \in \Pi_{p_e}(\mathbf{u}) \cap \partial\mathcal{B}_{p_e}$, such that the circle centered at $\mathbf{b}$ that also contains $\mathbf{o}$ is tangent to $\mathcal{S}^{\mathbf{o}}_{p_e}(\mathcal{U})$ at $\mathbf{s}^{\mathbf{o},\mathbf{u}}_{p_e}$, and contains no points of $\mathcal{S}^{\mathbf{o}}_{p_e}(\mathcal{U})$ in its interior.

A consequence of the geometric property stated in Proposition 4 is that, given a parametrization of unit vectors in $\mathbb{R}^n$, we will be able to derive a parametric characterization of $\partial\mathcal{B}_{p_e}$. The key insight from Figure 6 is that, given certain regularity assumptions, the vectors tangential to the set $\mathcal{S}^{\mathbf{o}}_{p_e}(\mathcal{U})$ and the ball $\mathcal{W}^{\mathbf{o}}(\mathbf{b})$ coincide at $\mathbf{s}^{\mathbf{o},\mathbf{u}}_{p_e}$. This will eventually let us derive a parametric representation of the set $\partial\mathcal{B}_{p_e}$ as a $(n-1)$-dimensional manifold. So now, motivated by the properties derived in the discrete scenario using tools from computational geometry, i.e. the Voronoi and

Delaunay tessellations, we will move to the continuous limit and study environmental contours in the context of differential geometry.

We will start by assuming that the set $\mathcal{S}^{\mathbf{o}}_{p_e}(\mathcal{U})$, viewed as a $(n-1)$-dimensional manifold embedded in $\mathbb{R}^n$, is differentiable. We recall that a m-dimensional manifold $\mathcal{S}$ in $\mathbb{R}^n$, for $m \leq n$, can be represented by a set of *charts* $\sigma_i : V_i \to \mathcal{S}$, where V_i are open non-empty subsets of $\mathbb{R}^m$. Any set of charts $\{\sigma_i, V_i\}_i$ that cover $\mathcal{S}$, i.e. $\mathcal{S} = \cup_i \sigma_i(V_i)$, is called an *atlas* of $\mathcal{S}$. We will in particular consider a regular parametrization of the unit $(n-1)$-sphere $\mathcal{U}$, by which we mean a set of charts $\{\sigma_i, V_i\}_i$ covering $\mathcal{U}$ where each σ_i is smooth and where the Jacobi matrix of σ_i has rank $n-1$ at any point in V_i. With the canonical alternative of spherical coordinates in mind, we will let $\{\mathbf{u}_i(\boldsymbol{\theta}) \mid \boldsymbol{\theta} \in \Theta_i\}_i$ denote an atlas of $\mathcal{U}$ with these properties. With some abuse of terminology, we will also refer to $\{\mathbf{u}_i(\boldsymbol{\theta}) \mid \boldsymbol{\theta} \in \Theta_i\}_i$ as a *regular parametrization* of $\mathcal{U}$. Given such a regular parametrization of $\mathcal{U}$, we will continue to construct corresponding parametrizations of $\mathcal{S}^{\mathbf{o}}_{p_e}(\mathcal{U})$ and eventually $\partial\mathcal{B}_{p_e}$. But first we will need a preliminary result given in Lemma 2 below.

Lemma 2 *Assume $\partial\mathcal{B}_{p_e}$ is a proper convex environmental contour with $\mathcal{B}_{p_e}$ defined as in (2), let $\mathbf{o} \in \mathcal{B}_{p_e} \setminus \partial\mathcal{B}_{p_e}$ and assume $\mathcal{S}^{\mathbf{o}}_{p_e}(\mathcal{U})$ is a differentiable manifold.*

If the pair $(\mathbf{a}, \mathbf{u})$, for some $\mathbf{a} \in \mathbb{R}^n$ and $\mathbf{u} \in \mathcal{U}$, satisfies the following

1. $\|\mathbf{a} - \mathbf{o}\| = \left\|\mathbf{s}^{\mathbf{o},\mathbf{u}}_{p_e} - \mathbf{a}\right\|$, *and*
2. $(\mathbf{s}^{\mathbf{o},\mathbf{u}}_{p_e} - \mathbf{a})$ *is orthogonal to* $\mathcal{S}^{\mathbf{o}}_{p_e}(\mathcal{U})$ *at* $\mathbf{s}^{\mathbf{o},\mathbf{u}}_{p_e}$,

then $\{\mathbf{a}\} = \Pi_{p_e}(\mathbf{u}) \cap \partial\mathcal{B}_{p_e}$.

In the proof of Lemma 2, given in Appendix E, we also show that for any $\mathbf{u} \in \mathcal{U}$, $\Pi_{p_e}(\mathbf{u}) \cap \partial\mathcal{B}_{p_e}$ is a singleton set, as $\Pi_{p_e}(\mathbf{u}) \cap \partial\mathcal{B}_{p_e}$ is nonempty when $\partial\mathcal{B}_{p_e}$ is a proper convex environmental contour and the pair $(\mathbf{b}, \mathbf{u})$ satisfies the conditions in Lemma 2 for any $\mathbf{b} \in \Pi_{p_e}(\mathbf{u}) \cap \partial\mathcal{B}_{p_e}$. This means that the set $\mathcal{B}_{p_e}$ has no "flat parts", and that $\mathcal{B}_{p_e}$ is in fact strictly convex. But besides this, the conditions in Lemma 2 will also serve as a more practical criterion to verify that a given mapping (soon to be given explicitly) gives a representation of the environmental contour $\partial\mathcal{B}_{p_e}$. This result is summarised in Proposition 5 below, with a proof given in Appendix F.

Proposition 5 *Let $F : \mathcal{U} \to \mathbb{R}^n$ be a mapping such that the assumptions and conditions of Lemma 2 hold for any pair $(F(\mathbf{u}), \mathbf{u})$. Then $F(\mathcal{U}) = \partial\mathcal{B}_{p_e}$.*

Now, the next step is to introduce a specific parametrization of $\partial\mathcal{B}_{p_e}$ that we will use Proposition 5 to verify. We will achieve this by mapping a parametrization of the unit $(n-1)$-sphere $\mathcal{U}$ to a parametrization of $\partial\mathcal{B}_{p_e}$. This idea has been explored in [37,32] for the 2-dimensional case using the parametrization $\mathbf{u}(\theta) = (\cos(\theta), \sin(\theta))$, where also the existence of a proper convex environmental contour is determined from properties related to the parametrized percentile function $C_{p_e}(\theta) = C_{p_e}(\mathbf{u}(\theta))$. In the following we will extend this to the n-dimensional case.

Let $\{\mathbf{u}_i(\boldsymbol{\theta}) \mid \boldsymbol{\theta} \in \Theta_i\}_i$ be the regular parametrization of $\mathcal{U}$ introduced previously. Suppressing the index i, for any chart $\mathbf{u}(\boldsymbol{\theta}) : \Theta \to \mathcal{U}$ we define the functions $C^{\mathbf{o}}_{p_e}(\boldsymbol{\theta})$ and $\mathbf{s}^{\mathbf{o}}_{p_e}(\boldsymbol{\theta})$ accordingly,

$$C^{\mathbf{o}}_{p_e}(\boldsymbol{\theta}) = C^{\mathbf{o}}_{p_e}(\mathbf{u}(\boldsymbol{\theta})) : \Theta \to \mathbb{R},$$
$$\mathbf{s}^{\mathbf{o}}_{p_e}(\boldsymbol{\theta}) = \mathbf{o} + 2C^{\mathbf{o}}_{p_e}(\boldsymbol{\theta})\mathbf{u}(\boldsymbol{\theta}) : \Theta \to \mathbb{R}^n,$$

where we will assume that both $\mathbf{u}(\boldsymbol{\theta})$ and $C^{\mathbf{o}}_{p_e}(\boldsymbol{\theta})$ are continuously differentiable as functions of $\boldsymbol{\theta}$, and let $\nabla_{\boldsymbol{\theta}}$ denote the Jacobian. That is, for functions $\mathbf{f} : \Theta \to \mathbb{R}^m$, $\nabla_{\boldsymbol{\theta}}\mathbf{f}$ is the $m \times (n-1)$ matrix with entries $[\nabla_{\boldsymbol{\theta}}\mathbf{f}]_{i,j} = \partial\mathbf{f}_i/\partial\boldsymbol{\theta}_j$. The assumption that $\mathbf{u}(\boldsymbol{\theta})$ is a *regular* parametrization means that we also assume that $\nabla_{\boldsymbol{\theta}}\mathbf{u}(\boldsymbol{\theta})$ has rank $n-1$ for any $\boldsymbol{\theta} \in \Theta$.

Theorem 1 (Representation of proper convex environmental contours) *Assume the n-dimensional random variable $\mathbf{X}$ admits a proper convex environmental contour $\partial\mathcal{B}_{p_e}$ with respect to a target probability $p_e \in (0, 0.5)$, and assume that the p_e-level percentile function $C_{p_e}(\mathbf{u})$ is k-times continuously differentiable on the unit $(n-1)$-sphere for $k \geq 1$.*

Then $\mathcal{B}_{p_e}$ is strictly convex, and $\partial\mathcal{B}_{p_e}$ is a $(k-1)$-times differentiable manifold. Furthermore, if $\{\mathbf{u}_i(\boldsymbol{\theta}) \mid \boldsymbol{\theta} \in \Theta_i\}_{i=1}^m$ is a regular parametrization of the unit $(n-1)$-sphere, then an atlas of $\partial\mathcal{B}_{p_e}$ is obtained by $\{\mathbf{b}_i(\boldsymbol{\theta}) \mid \boldsymbol{\theta} \in \Theta_i\}_{i=1}^m$, where $\mathbf{b}_i(\boldsymbol{\theta})$ is obtained from $\mathbf{u}_i(\boldsymbol{\theta})$ using the following relation:

$$\mathbf{b}(\boldsymbol{\theta}) = C_{p_e}(\boldsymbol{\theta})\mathbf{u}(\boldsymbol{\theta}) + \nabla_{\boldsymbol{\theta}}\mathbf{u}(\boldsymbol{\theta})\eta^{-1}(\boldsymbol{\theta})(\nabla_{\boldsymbol{\theta}}C_{p_e}(\boldsymbol{\theta}))^T, \tag{10}$$

and where $\eta(\boldsymbol{\theta}) = \nabla_{\boldsymbol{\theta}}\mathbf{u}(\boldsymbol{\theta})^T\nabla_{\boldsymbol{\theta}}\mathbf{u}(\boldsymbol{\theta})$ *is the metric tensor of the* $(n-1)$*-sphere induced by the parametrization* $\mathbf{u}(\boldsymbol{\theta})$*.*

The proof of Theorem 1 is given in Appendix G. Note that Theorem 1 gives an analytic expression for the environmental contour (i.e. $\mathbf{b}_i(\boldsymbol{\theta})$) in terms of the p_e-level percentile function $C_{p_e}(\boldsymbol{\theta})$. Thus, given a specific parametrization and a differentiable approximation of $C_{p_e}(\boldsymbol{\theta})$ it is possible to compute $\mathbf{b}(\boldsymbol{\theta})$ directly, as an alternative to explicitly constructing a Voronoi cell as described in section 4. One common parametrization in the n-dimensional case is given by $\mathbf{u}(\boldsymbol{\theta}) = (u_0, u_1, \ldots, u_{n-1})$ with $u_i = \cos\theta_i \prod_{j=0}^{i-1}\sin\theta_j$ for $i = 0, 1, \ldots, n-2$ and $u_{n-1} = \prod_{j=0}^{n-2}\sin\theta_j$, where $\theta_i \in [0, \pi)$ for $i = 1, 2, \ldots, n-2$ and $\theta_{n-2} \in [0, 2\pi)$. The corresponding induced metric tensor has entries $\eta_{0,0} = 1$, $\eta_{i,i} = \prod_{j=0}^{i-1}\sin\theta_j{}^2$ for $i = 0, 1, \ldots, n-2$ and $\eta_{i,j} = 0$ if $i \neq j$.

It would be desirable to have a criterion for $C_{p_e}(\boldsymbol{\theta})$ that guarantees that $\mathbf{b}_i(\boldsymbol{\theta})$ represent a proper environmental contour. To obtain such a criterion, we will need a couple of intermediate results given in the following Lemmas.

Lemma 3 *The random variable* $\mathbf{X}$ *admits a proper convex environmental contour with respect to* $p_e \in (0, 0.5)$ *if and only if the following holds:*

For any $\mathbf{u}' \in \mathcal{U}$*, there exists some* $\mathbf{o} \in \Pi_{p_e}(\mathbf{u}')$ *such that* $C^{\mathbf{o}}_{p_e}(\mathbf{u}) \geq 0$ *for all* $\mathbf{u} \in \mathcal{U}$*.*

Lemma 4 *Assume the percentile function* $C_{p_e}(\boldsymbol{\theta})$ *is twice differentiable and that* $\mathbf{u}(\boldsymbol{\theta}) : \Theta \to \mathcal{U}$ *is regular (*$\nabla\mathbf{u}(\boldsymbol{\theta})$ *exists and has full rank for all* $\boldsymbol{\theta}$*). Let* $\mathbf{b}(\boldsymbol{\theta})$ *be defined as in* (10)*. Then*

$$\mathbf{u}(\boldsymbol{\theta})^T\mathbf{b}(\boldsymbol{\theta}) = C_{p_e}(\boldsymbol{\theta}) \text{ and } \mathbf{u}(\boldsymbol{\theta})^T\nabla\mathbf{b}(\boldsymbol{\theta}) = \mathbf{0}$$

for all $\boldsymbol{\theta} \in \Theta$*. This means that* $\Pi_{p_e}(\boldsymbol{\theta})$ *is tangential to* $\mathbf{b}(\Theta)$ *at the point* $\mathbf{b}(\boldsymbol{\theta})$*.*

Lemma 3 comes as a consequence of Lemma 1, and the proof is given in Appendix H. In Appendix I we present the proof of Lemma 4, which states that for any $\boldsymbol{\theta}$, the hyperplane $\Pi_{p_e}(\boldsymbol{\theta})$ is tangential to $\mathbf{b}(\Theta)$ at the point $\mathbf{b}(\boldsymbol{\theta})$.

Armed with these results we can prove the following criteria for existence.

Theorem 2 (Existence of proper convex environmental contours) *Let* $\mathbf{X}$ *be any* n*-dimensional random variable where the percentile function* $C_{p_e}(\cdot)$ *is differentiable on the unit* $(n-1)$*-sphere. Let* $\{\mathbf{u}_i(\boldsymbol{\theta}) \mid \boldsymbol{\theta} \in \Theta_i\}_{i=1}^m$ *be a regular parametrization of the unit* $(n-1)$*-sphere, and define for any* $\mathbf{u}(\boldsymbol{\theta}) = \mathbf{u}_i(\boldsymbol{\theta})$ *the function*

$$\kappa(\boldsymbol{\theta}|\boldsymbol{\theta}') = C^{\mathbf{b}(\boldsymbol{\theta}')}_{p_e}(\boldsymbol{\theta}) = C_{p_e}(\boldsymbol{\theta}) - \mathbf{u}(\boldsymbol{\theta}) \cdot \mathbf{b}(\boldsymbol{\theta}'),$$

where $C_{p_e}(\boldsymbol{\theta}) = C_{p_e}(\mathbf{u}(\boldsymbol{\theta}))$ *and* $\mathbf{b}(\boldsymbol{\theta}')$ *is given by* (10) *with* $\boldsymbol{\theta} = \boldsymbol{\theta}'$*.*

Then the following are equivalent:

1. $\mathbf{X}$ *admits a proper convex environmental contour.*
2. *The hypersurface given by the parametrization* $b(\boldsymbol{\theta})$ *in* (10) *is the boundary of a closed convex set.*
3. $\kappa(\boldsymbol{\theta}|\boldsymbol{\theta}') \geq 0$ *for all* $\mathbf{u}(\boldsymbol{\theta}) = \mathbf{u}_i(\boldsymbol{\theta}), \boldsymbol{\theta}, \boldsymbol{\theta}' \in \Theta_i$*, and* $i = 1, \ldots, m$*.*
4. $\kappa(\boldsymbol{\theta}|\boldsymbol{\theta}')$ *attains its global minimum at* $\boldsymbol{\theta} = \boldsymbol{\theta}'$ *for all* $\mathbf{u}(\boldsymbol{\theta}) = \mathbf{u}_i(\boldsymbol{\theta}), i = 1, \ldots, m$*.*

The proof of Theorem 2 is provided in Appendix J. In the 2-dimensional case with polar coordinates, one can also show that existence is equivalent to the criterion that $C_{p_e}(\theta) + C''_{p_e}(\theta) > 0$ for all $\theta \in [0, 2\pi)$ (see Theorem 3.13 in [32]). As a consequence of Theorem 2, we can obtain the following similar result stated in Corollary 2 below.

Corollary 2 *Assume the* n*-dimensional random variable* $\mathbf{X}$ *admits a proper convex environmental contour, and that* $C_{p_e}(\boldsymbol{\theta})$ *is twice differentiable. Then* $Hess(C_{p_e}(\boldsymbol{\theta})) + \eta(\boldsymbol{\theta})C_{p_e}(\boldsymbol{\theta})$ *is positive semi-definite for all* $\boldsymbol{\theta} \in \Theta$*, where* $Hess(\cdot)$ *is the Hessian operator on the* $(n-1)$*-sphere and* $\eta(\boldsymbol{\theta})$ *is the* $(n-1)$*-sphere metric tensor.*

The proof of Corollary 2 is given in Appendix K. Note that the metric tensor on the unit circle is simply $\eta = 1$, so the 2-dimensional version of Corollary 2 states that $C_{p_e}(\theta) + C''_{p_e}(\theta) \geq 0$. As a stronger version of the statement holds in the 2-dimensional case, we might conjecture that the criterion in Corollary 2 with strict positive definiteness could hold as a necessary condition, but we have currently not explored this further in any detail.

6 Practical application of the Voronoi method for environmental contour approximation

In Section 4 we outlined a potential procedure for approximating environmental contours using the Voronoi-representation. Based on this idea, we present the steps involved in Algorithm 3 below, followed up by a discussion on how each step may be implemented in practice.

Algorithm 3 *Approximating $\mathcal{B}_{p_e}$ using the Voronoi method*

1. *Select a set of unit vectors $U = \{\mathbf{u}_j\}_{j=1}^M$.*
2. *Estimate $\widehat{C}_{p_e}(\mathbf{u}_j) \approx C_{p_e}(\mathbf{u}_j)$ for each $j = 1, \dots, M$.*
3. *Compute $\widehat{\mathcal{S}}^{\mathbf{o}}_{p_e}(U)$, using $\widehat{C}^{\mathbf{o}}_{p_e}(\mathbf{u}_j)$ in (9), for some $\mathbf{o} \in \mathcal{B}_{p_e} \setminus \partial\mathcal{B}_{p_e}$.*
4. *Compute the approximation $\widehat{\mathcal{B}}_{p_e} = Vor(\mathbf{o}, \widehat{\mathcal{S}}^{\mathbf{o}}_{p_e}(U))$.*
5. *Check that each point in $\widehat{\mathcal{S}}^{\mathbf{o}}_{p_e}(U)$ is connected with $\mathbf{o}$ in the Delaunay triangulation of the point set $\{\mathbf{o}\} \cup S^{\mathbf{o}}_{p_e}(U)$.*

Step 1: The algorithm will produce finer approximations as more unit vectors are included. However, the main computational burden is usually related to the estimation of $C_{p_e}(\mathbf{u}_j)$ for each unit vector, so the number of unit vectors is often decided by the desired run-time of the entire algorithm. In applications such as design of marine structures, there might be knowledge related to which directions that are the most informative, and the set U might be chosen on this basis. Alternatively, a uniform selection may be applied. One way to generate uniform random samples from the unit $(n-1)$-sphere is to let $\mathbf{u}_j = \mathbf{v}_j / \|\mathbf{v}_j\|$ where $\mathbf{v}_j = (v_{1,j}, \dots, v_{n,j})$ and all $v_{1,j}$ are i.i.d. Gaussian [49].

Step 2: In practice, we might not be able to compute $C_{p_e}(\mathbf{u}_j)$ exactly. However, this can be estimated based on a finite number of Monte Carlo samples from the joint distribution, in the same way as outlined in [35,37]. The estimation error will depend on the sample size and may in principle be reduced to an acceptable level by increasing the number of samples, or for example using the importance sampling scheme proposed in [36]. Moreover, if one were to apply conservative estimates, i.e. $\widehat{C}_{p_e}(\mathbf{u}_j) \geq C_{p_e}(\mathbf{u}_j)$, this would produce a conservative (larger) environmental contour approximation as well.

Step 3: In order to compute $\widehat{\mathcal{S}}^{\mathbf{o}}_{p_e}(U)$, we first need some point of reference $\mathbf{o}$ from the interior of $\mathcal{B}_{p_e}$. The criterion that $C^{\mathbf{o}}_{p_e}(\mathbf{u}) > 0$ for any $\mathbf{u} \in \mathcal{U}$ (see Lemma 1) can be used to identify if the selected origin $\mathbf{o}$ is not in the interior of $\mathcal{B}_{p_e}$. We can then also observe that, in the case where we want to replace the origin $\mathbf{o}$ with some new point $\mathbf{o}^*$, the new set $\mathcal{S}^{\mathbf{o}^*}_{p_e}$ can be computed using that $C^{\mathbf{o}^*}_{p_e}(\mathbf{u}) = C^{\mathbf{o}}_{p_e}(\mathbf{u}) + \mathbf{u} \cdot (\mathbf{o} - \mathbf{o}^*)$, and hence

$$\mathbf{s}^{\mathbf{o}^*,\mathbf{u}}_{p_e} = \mathbf{s}^{\mathbf{o},\mathbf{u}}_{p_e} + 2\mathbf{u} \cdot (\mathbf{o} - \mathbf{o}^*)\mathbf{u} - (\mathbf{o} - \mathbf{o}^*).$$

This means that the estimates $\widehat{C}_{p_e}(\mathbf{u}_j)$ can be reused, as going from $\widehat{\mathcal{S}}^{\mathbf{o}}_{p_e}(U)$ to $\widehat{\mathcal{S}}^{\mathbf{o}^*}_{p_e}(U)$ is a simple linear transformation. We may also note the geometric interpretation, by observing that the added term $2\mathbf{u} \cdot (\mathbf{o} - \mathbf{o}^*)\mathbf{u} - (\mathbf{o} - \mathbf{o}^*)$ is the reflection of the point $(\mathbf{o} - \mathbf{o}^*)$ with respect to the unit vector $\mathbf{u}$. As both checking whether $C^{\mathbf{o}}_{p_e}(\mathbf{u}) > 0$ and moving the origin $C^{\mathbf{o}}_{p_e}(\mathbf{u}) \to C^{\mathbf{o}^*}_{p_e}(\mathbf{u})$ are cheap computationally, one could derive an iterative procedure to determine $\mathbf{o}$. Alternatively, finding the point $\mathbf{o}$ with maximal distance to all hyperplanes under the restriction that $C^{\mathbf{o}}_{p_e}(\mathbf{u}_j) > 0$, which is equivalent to $C_{p_e}(\mathbf{u}_j) > \mathbf{u}_j \cdot \mathbf{o}$, for each $j = 1, \dots, M$ can be solved by linear programming. In our implementation, the geometric median of a set of samples from the joint distribution of $\mathbf{X}$ (the ones used to estimate $C_{p_e}(\mathbf{u}_j)$ in Step 2) was selected as the origin $\mathbf{o}$. This choice of $\mathbf{o}$ will with high probability lie inside $\mathcal{B}_{p_e}$ for any $p_e > 0.5$, and in our experiments we did not find the need to iterate further beyond this initial guess.

Step 4: Some of the motivation for this paper comes from the fact that the Voronoi tessellation is a well studied object. As a result, a wide range of software and programming languages come with efficient procedures for computing Voronoi cells, including Python/Scipy, R, Wolfram Language/Mathematica, Matlab and Octave. Moreover, Voronoi algorithms work in arbitrary dimensions, which is what makes the proposed algorithm agnostic to the dimensionality of $\mathbf{X}$.

Step 5: This check comes as a consequence of Proposition 3 and Corollary 1. There are two scenarios that may cause this check to fail. 1) When the selected probability distribution does not admit a proper convex environmental contour with respect to the chosen target probability,

and 2) when the percentile function $C_{p_e}(\mathbf{u})$ is estimated with error. In the case where the check fails due to noise in the estimates $\widehat{C}_{p_e}(\mathbf{u}_j)$, we can make refinements based on the relevant unit vectors. For instance, if it is found that the point $\hat{\mathbf{s}}_k \in \widehat{\mathcal{S}}^{\mathbf{o}}_{p_e}(U)$ corresponding to unit vector $\mathbf{u}_k$ is not connected with $\mathbf{o}$, the estimates $\widehat{C}_{p_e}(\mathbf{u}_j)$ can be refined for relevant indices j. The relevant indices here, besides $j = k$, are the ones corresponding to points $\hat{\mathbf{s}}_j$ affecting the Delaunay triangulation in the vicinity of $\hat{\mathbf{s}}_k$, which are the points connected with $\hat{\mathbf{s}}_k$ and the neighbouring Delaunay simplices. With reference to the previous step, we also note that the task of obtaining the Delaunay triangulation usually "comes for free", in the sense that available algorithms used to obtain the Voronoi tessellation do this by computing the Delaunay triangulation and taking the dual.

The goal of this numerical procedure presented in Algorithm 3 is to provide a good approximation in the case where a proper convex environmental contour exists. In the case where a proper convex environmental contour *does not* exist, one might still be interested in finding a *valid* convex environmental contour that is "as small as possible". That is, a convex set where the exceedance probability of each supporting half-space is less than or equal to p_e (where it cannot be equal to p_e for all supporting half-spaces as no *proper* convex environmental contour exists). We will end this section with a modified version of the algorithm to accommodate this scenario.

The contour $\partial\mathcal{B}_{p_e}$ corresponding to the boundary of a Voronoi cell $Vor(\mathbf{o}, \mathcal{S}^{\mathbf{o}}_{p_e}) = \bigcap_{\mathbf{u}\in U} \Pi^{-}_{p_e}(\mathbf{u})$ is only a valid and proper environmental contour if $\partial\mathcal{B}_{p_e} \cap \Pi^{-}_{p_e}(\mathbf{u}) \neq \emptyset \ \forall \mathbf{u} \in U$. Otherwise, it is invalid. We may however use an *invalid* Voronoi contour to create a *valid improper* contour by the following algorithm:

Algorithm 4 *Let V be a Voronoi contour computed by Algorithm 3 based on a set of unit vectors U.*

1. *Initialise $Z = V$.*
2. *For each direction $\mathbf{u} \in U$:*
   (a) *Find the point $\mathbf{v}' \in V$ that is furthest out in direction $\mathbf{u}$, i.e. $\mathbf{v}' = \underset{\mathbf{v}\in V}{\operatorname{argmax}}\{\mathbf{v} \cdot \mathbf{u}\}$.*
   (b) *Compute the projection of $\mathbf{v}'$ onto the plane $\Pi_{p_e}(\mathbf{u})$, i.e. $\mathbf{z} = \mathbf{v}' + (C_{p_e}(\mathbf{u}) - \mathbf{v}' \cdot \mathbf{u})\mathbf{u}$.*
   (c) *Update $Z \to Z \cup \{\mathbf{z}\}$.*
3. *Compute the convex hull of Z. This is the corrected Voronoi contour.*

The algorithm above guarantees a valid environmental contour with respect to U, because it intersects all the hyperplanes $\Pi^{-}_{p_e}(\mathbf{u})$ $\forall \mathbf{u} \in U$ by construction. The projection algorithm is illustrated in figure 7.

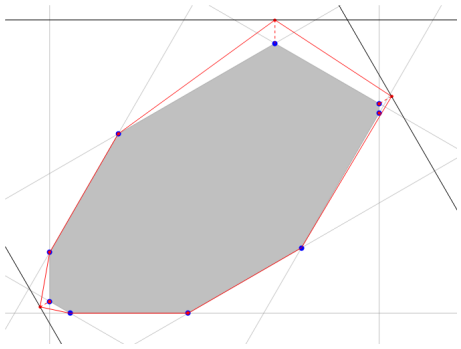

Fig. 7: Illustration of algorithm 4 to construct a valid environmental contour (red).

Figure 8 shows two examples using the above algorithms and also the direct method presented in [35]. First, a scenario where a proper convex environmental contour exists, and then a scenario where a proper environmental contour does not exist. The top row corresponds to a centered bivariate normal distribution with covariance $0.16 \cdot [1\ 0.5; 0.5\ 1]$, and the bottom row represents a Gaussian mixture; $\mathbf{X} = 0.8\mathbf{X}_1 + 0.1\mathbf{X}_2 + 0.1\mathbf{X}_3$ where $\mathbf{X}_1 \sim \mathcal{N}([0\ 0]^T, 0.16I)$, $\mathbf{X}_2 \sim \mathcal{N}([0.5\ 1]^T, 0.04I)$ and $\mathbf{X}_3 \sim \mathcal{N}([-0.5\ 1]^T, 0.04I)$. The contours are computed with $p_e = 0.15$.

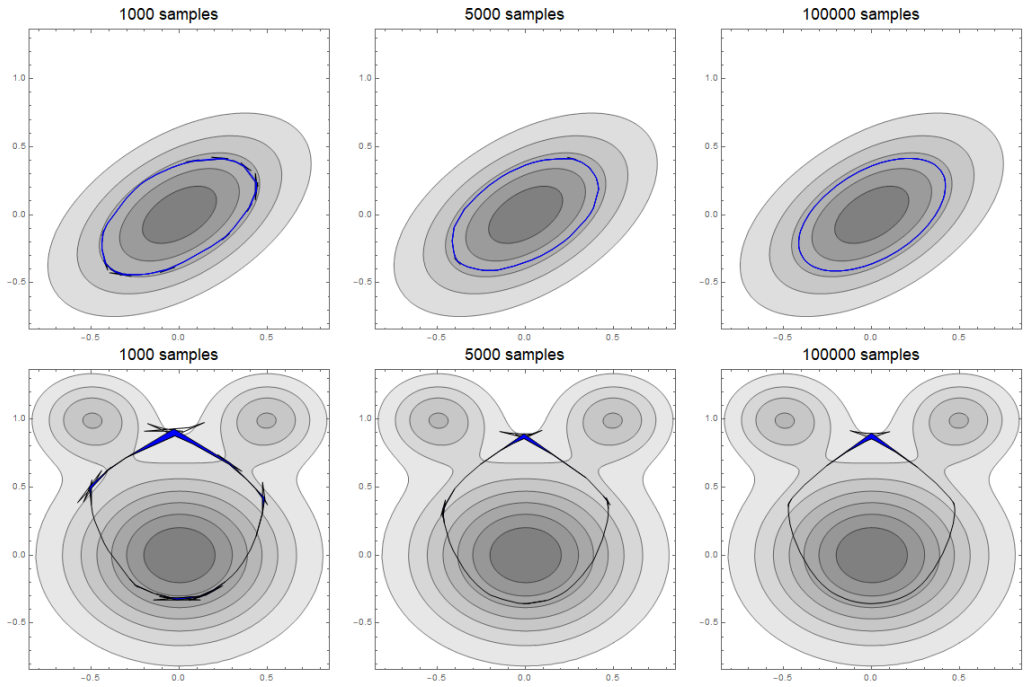

Fig. 8: Top: Contours for a multinormal distribution, constructed using the direct method of [35]. The loops disappear as the number of samples increased, indicating that the loops is a sampling issue. Bottom: Contours for a multimodal distribution constructed using the direct method of [35]. The top loops do not disappear as the number of samples increase, indicating that the loops is a feature of the underlying distribution (i.e. the distribution does not admit a proper convex contour for the selected target probability).

7 Examples

7.1 2D example

To illustrate the Voronoi approach in two dimensions, we use the same example as [35]. The environmental variables of interest are the significant wave height, H_S, and the zero-upcrossing wave period, T_Z. Their joint distribution is modelled using a conditional modelling approach [8, 11], and can be expressed as

$$f_{H,T}(h,t) = f_H(h) f_T(t|h).$$

Here, $f_H(h)$ is a 3-parameter Weibull distribution for significant wave height, with scale parameter α, shape parameter β, and location parameter γ. The term $f_T(t|h)$ is a conditional log-normal distribution for wave period, where the model parameters are functions of significant wave height, as outlined in e.g. [23, 75], i.e.

$$\mu_T(h) = E\left(\ln T_Z | H_S = h\right) = a_1 + a_2 h^{a_3}$$
$$\sigma_T(h) = sd\left(\ln T_Z | H_S = h\right) = b_1 + b_2 e^{b_3 h}.$$

The parameter values used are listed in Table 1.

Table 1: Parameters assumed for the bivariate distribution of H_S and T_S.

3-p Weibull (H_S)	α	β	γ
	2.776	1.471	0.8888
Conditional log-normal (T_Z)	i = 1	i = 2	i = 3
a_i	0.1000	1.4890	0.1901
b_i	0.0400	0.1748	-0.2243

Figure 9 shows comparisons of results for different methods. The number of samples that the contours are based on is varied in the rows, but the samples are identical within each row. The number of unit vectors used to compute the contours is varied in the columns.

The direct sampling method of [35] is drawn in black. This method does not guarantee convex contours, but sometimes produce loops. Keeping the samples fixed, the loops tend to be larger as the number of unit vectors increase, which is undesirable. However, the loops tend to get smaller with increased number of samples. The convex hull of the black contours are drawn in red. Note that for the same number of samples, these red contours tend to get larger when the number of directions is increased, due to the larger loops.

Contours based on the Voronoi method are shown in blue. More precisely, blue regions are plotted, where the inner boundary correspond to the simple Voronoi method (i.e. Algorithm 3), and the outer boundary correspond to the corrected Voronoi method (i.e. Algorithm 4). Note that, unlike the other methods, the contours produced by the Voronoi methods do not diverge as the number of directions is increased. We also see that the shaded region is generally thin, indicating that the simple Voronoi method is a good approximation to the 'true' environmental contour. The inset shows the error, i.e. the difference between the two Voronoi methods in the various directions. The directions with high error corresponds to directions where the direct method of [35] produces loops, i.e. the Voronoi method provides a warning for directions where more sampling may be needed.

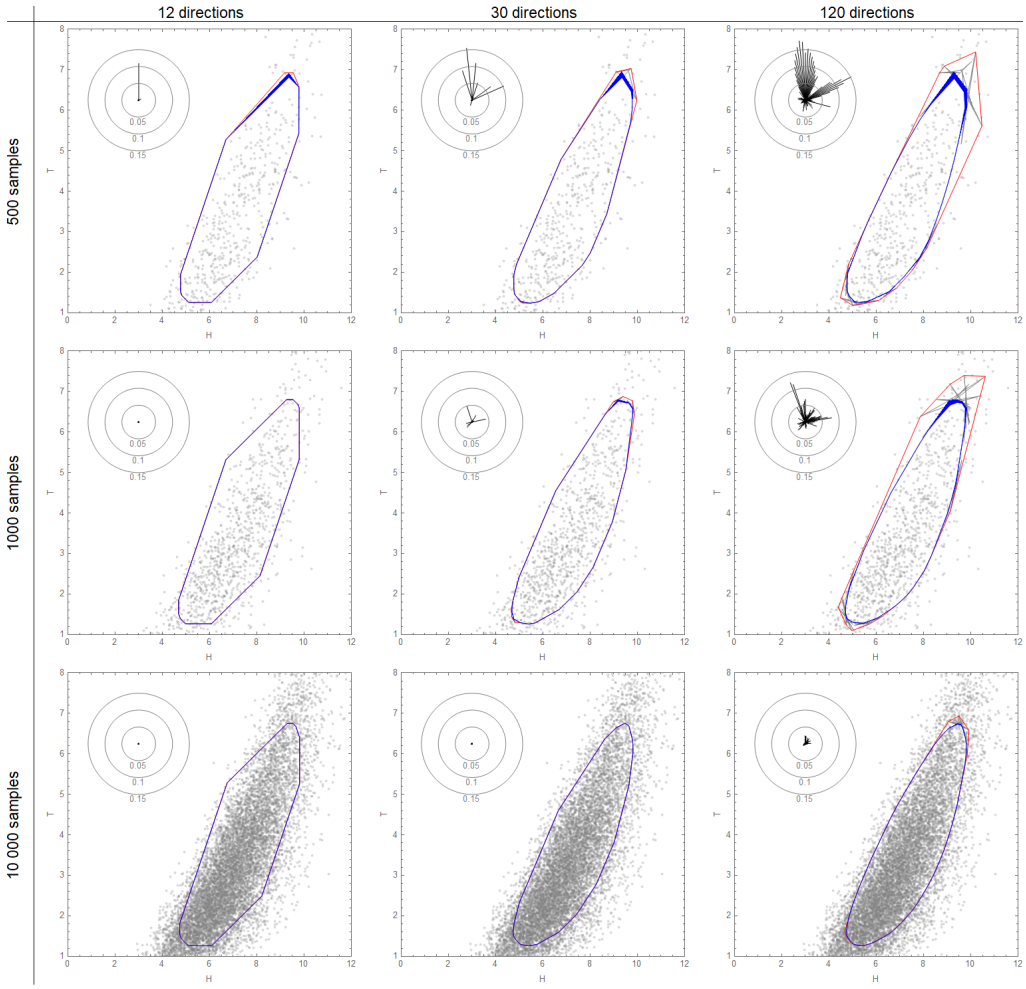

Fig. 9: Comparison of results, for $p_e = 0.05$. The samples that contours are computed from are shown in grey. The grey curves represent the direct sampling method of [35] (visible only in the third column). The red curves represent the convex hull of the grey curves. The blue regions represent the Voronoi methods; the inner boundary correspond to the simple Voronoi method, and the outer boundary correspond to the corrected Voronoi method. The insets show the error in different directions, i.e. the difference between the simple and corrected Voronoi methods.

7.2 3D example

To illustrate the Voronoi approach in three dimensions, we include an example from [71]. The environmental variables of interest are the significant wave height, H_S, the zero-upcrossing wave period, T_Z, and the 10-minute mean wind speed at a particular height, U_{10}. Their joint distribution is modelled using a conditional modelling approach [8,11], and can be expressed as

$$f_{H,T,U}(h,t,u) = f_H(h) f_T(t|h) f_U(u|h).$$

Here $f_H(h)$ is a 3-parameter Weibull distribution for significant wave height, with scale parameter α, shape parameter β, and location parameter γ.

The term $f_T(t|h)$ is a conditional log-normal distribution for wave period, where the model parameters are a function of significant wave height as outlined in e.g. [23,75], i.e.

$$\mu_T(h) = E\left(\ln T_Z | H_S = h\right) = a_1 + a_2 h^{a_3}$$
$$\sigma_T(h) = sd\left(\ln T_Z | H_S = h\right) = b_1 + b_2 e^{b_3 h}.$$

The parameters a_i, b_i, $i = 1,2,3$ are estimated from data.

$f_U(u|h)$ is a conditional 2-parameter Weibull distribution with parameters modelled as functions of significant wave height as suggested by [23,10,9]. The scale parameter, λ_U, and shape parameter, κ_U, are modelled as

$$\lambda_U(h) = c_1 + c_2 h^{c_3}$$
$$\kappa_U(h) = d_1 + d_2 h^{d_3}.$$

For the significant wave height and wave period, parameters corresponding to average world wide operations of ships according to appendix C of [23] are assumed, as summarised in Table 2. For the conditional distribution of wind speed, the average sectoral parameters reported in [10,9] will be assumed, as summarised in Table 2. It is noted that the parameter d_3 is omitted in [10], so this is simply set to 1 in this study.

Figure 10 shows the result of applying the Voronoi methods (simple and corrected) to the example described above. As can be seen, the simple method and corrected method are very similar, indicating that the simple Voronoi method is a good approximation for the 'true' environmental contour.

Table 2: Parameters assumed for the trivariate distribution of H_S, T_S and U_{10}.

3-p Weibull (H_S)		α	β	γ
average World wide trade		1.798	1.214	0.856
Conditional log-normal (T_Z)		i = 1	i = 2	i = 3
average World wide trade	a_i	-1.010	2.847	0.075
	b_i	0.161	0.146	-0.683
Conditional 2-p Weibull (U_{10})		i = 1	i = 2	i = 3
average directional sector	c_i	2.58	0.12	1.60
	d_i	4.6	2.05	1

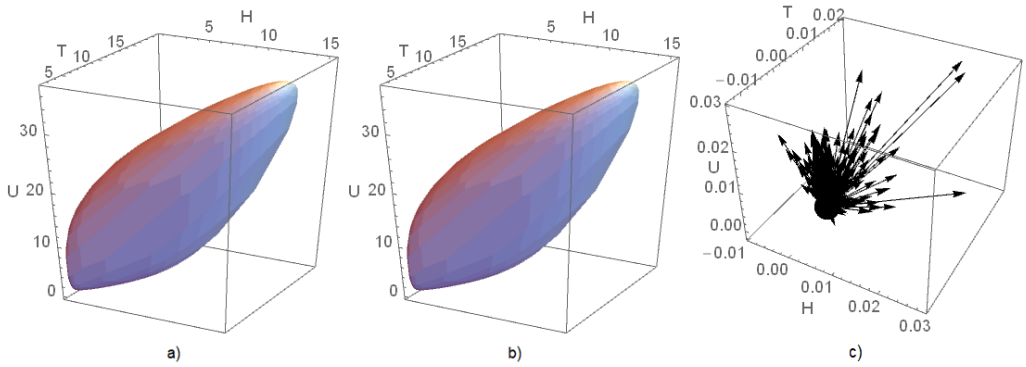

Fig. 10: a) Approximate (invalid) environmental contour for 3D example, computed using the simple Voronoi method (i.e. Algorithm 3). b) Valid (improper) environmental contour for 3D example, computed using the corrected Voronoi method (i.e. Algorithm 4). c) Difference between the corrected and simple Voronoi methods, showing that the simple method gives good approximation to a valid environmental contour.

8 Concluding remarks

In this paper, a novel algorithm for constructing environmental contours has been presented, based on a geometric interpretation of environmental contours as Voronoi cells. One advantage of this approach is that many software libraries exist for Voronoi cell computation, making the algorithm simple to implement. Another advantage is that the Voronoi method also makes it easy to compute environmental contours in higher than two dimensions. The Voronoi environmental contours are not guaranteed to be proper, but with a simple modification to the algorithm, valid environmental contours can always be constructed from improper Voronoi environmental contours.

The Voronoi geometric interpretation also has given new intuition and theoretical insights about environmental contours, including representation and existence theorems for proper convex environmental contours. The presented analytical formula provides another alternative algorithm to compute environmental contours. Interestingly, this formula has an analogy in shadow systems and can be interpreted as an inverse Gauss map [66,21,50]. Further exploration of this correspondence between environmental contours and shadow functions could potentially reveal new insights in both domains, and potentially provide some information on the class of random variables for which proper environmental contours exist.

Acknowledgements This work has been supported by grant 276282 from the Research Council of Norway (RCN) and DNV Group Research and Development. Parts of the work has also been carried out within the research project ECSADES, with support from RCN under the MARTEC II ERA-NET initiative; project no. 249261/O80.

Data availability The examples in this article are based on simulated data. All parameters needed to reproduce the examples are provided in the article.

Appendices

A Proof of Lemma 1

Proving the first statement is trivial, as $\mathbf{x} \in \mathcal{B}_{p_e}$ by definition means that $\mathbf{u} \cdot (\mathbf{x} - \mathbf{o}) \leq C^{\mathbf{o}}_{p_e}(\mathbf{u})$ for any $\mathbf{u} \in \mathcal{U}$. So, in particular, we have that $\mathbf{o} \in \mathcal{B}_{p_e} \Leftrightarrow 0 = \mathbf{u} \cdot (\mathbf{o} - \mathbf{o}) \leq C^{\mathbf{o}}_{p_e}(\mathbf{u})$.

To prove the second statement we use that

$$\mathbf{x} \in \mathcal{B}_{p_e} \setminus \partial\mathcal{B}_{p_e} \Rightarrow \mathbf{x} \in \bigcap_{\mathbf{u} \in \mathcal{U}} \left(\Pi^{-}_{p_e}(\mathbf{u}) \setminus \partial\Pi^{-}_{p_e}(\mathbf{u}) \right).$$

That is, a point $\mathbf{x}$ in the interior of $\mathcal{B}_{p_e}$ is also in the intersection of all interior half-spaces. Hence, $\mathbf{x} \in \{\mathbf{x} : \mathbf{u} \cdot (\mathbf{x} - \mathbf{o}) < C^{\mathbf{o}}_{p_e}(\mathbf{u})\}$ for all $\mathbf{u} \in \mathcal{U}$. And so by the same argument as above we have that $\mathbf{o} \in \mathcal{B}_{p_e} \setminus \partial\mathcal{B}_{p_e} \Rightarrow 0 = \mathbf{u} \cdot (\mathbf{o} - \mathbf{o}) < C^{\mathbf{o}}_{p_e}(\mathbf{u}) \; \forall \mathbf{u} \in \mathcal{U}$.

To prove the converse, we first observe that if $\mathbf{o} \in \partial\mathcal{B}_{p_e}$, then then there exists some $\mathbf{u}^* \in \mathcal{U}$ where $\mathbf{o} \in \partial\Pi^-_{p_e}(\mathbf{u}^*)$ (by the supporting hyperplane theorem) which means that $C^{\mathbf{o}}_{p_e}(\mathbf{u}^*) = 0$, and if $\mathbf{o} \notin \mathcal{B}_{p_e}$ then we have already shown that $C^{\mathbf{o}}_{p_e}(\mathbf{u}^*) < 0$ for some $\mathbf{u}^*$. Putting this together we get that $\mathbf{o} \notin \mathcal{B}_{p_e} \setminus \mathcal{B}_{p_e} \Rightarrow \exists \mathbf{u}^* \in \mathcal{U}$ s.t. $C^{\mathbf{o}}_{p_e}(\mathbf{u}^*) \leq 0$, and hence $C^{\mathbf{o}}_{p_e}(\mathbf{u}) > 0 \; \forall \mathbf{u} \in \mathcal{U} \Rightarrow \mathbf{o} \in \mathcal{B}_{p_e} \setminus \mathcal{B}_{p_e}$.

As for the final statement, we first recall that a point $\mathbf{x}$ is in $\mathrm{Vor}(\mathbf{o}, \mathcal{S}^{\mathbf{o}}_{p_e}(U))$ if and only if $\|\mathbf{x} - \mathbf{o}\| \leq \left\|\mathbf{x} - \mathbf{s}^{\mathbf{o},\mathbf{u}}_{p_e}\right\|$, or equivalently $\|\mathbf{x} - \mathbf{o}\|^2 \leq \left\|\mathbf{x} - \mathbf{s}^{\mathbf{o},\mathbf{u}}_{p_e}\right\|^2$, for any $\mathbf{u} \in U$. We first observe that

$$\left\|\mathbf{x} - \mathbf{s}^{\mathbf{o},\mathbf{u}}_{p_e}\right\|^2 = \left\|\mathbf{x} - \mathbf{o} - 2C^{\mathbf{o}}_{p_e}(\mathbf{u})\mathbf{u}\right\|^2 = \|\mathbf{x} - \mathbf{o}\|^2 + 4(C^{\mathbf{o}}_{p_e}(\mathbf{u}))^2 - 4C^{\mathbf{o}}_{p_e}(\mathbf{u})(\mathbf{x} - \mathbf{o}) \cdot \mathbf{u}, \tag{11}$$

and so,

$$\|\mathbf{x} - \mathbf{o}\|^2 \leq \left\|\mathbf{x} - \mathbf{s}^{\mathbf{o},\mathbf{u}}_{p_e}\right\|^2 \Leftrightarrow C^{\mathbf{o}}_{p_e}(\mathbf{u})(\mathbf{x} - \mathbf{o}) \cdot \mathbf{u} \leq (C^{\mathbf{o}}_{p_e}(\mathbf{u}))^2.$$

Hence, using the second statement of the Lemma, we have that if $\mathbf{o} \in \mathcal{B}_{p_e} \setminus \partial\mathcal{B}_{p_e}$ then $C^{\mathbf{o}}_{p_e}(\mathbf{u}) > 0$, and so $\|\mathbf{x} - \mathbf{o}\|^2 \leq \left\|\mathbf{x} - \mathbf{s}^{\mathbf{o},\mathbf{u}}_{p_e}\right\|^2 \Leftrightarrow (\mathbf{x} - \mathbf{o}) \cdot \mathbf{u} \leq C^{\mathbf{o}}_{p_e}(\mathbf{u})$ for any $\mathbf{u} \in U$ which completes the proof. □

B Proof of Proposition 2

First we recall that by definition $\mathcal{B}_{p_e} = \bigcap_{\mathbf{u}\in\mathcal{U}} \Pi^-_{p_e}(\mathbf{u})$. Using Lemma 1 we then have $\mathcal{B}_{p_e} = \mathrm{Vor}(\mathbf{o}, \mathcal{S}^{\mathbf{o}}_{p_e}(\mathcal{U}))$, and also $\mathrm{Vor}(\mathbf{o}, \mathcal{S}^{\mathbf{o}}_{p_e}(U_i)) = \bigcap_{\mathbf{u}\in U_i} \Pi^-_{p_e}(\mathbf{u})$ for $i = 1, 2$.

Since $U_1 \subseteq U_2 \subseteq \mathcal{U}$ the proof is completed by observing that

$$\bigcap_{\mathbf{u}\in\mathcal{U}} \Pi^-_{p_e}(\mathbf{u}) \subseteq \bigcap_{\mathbf{u}\in U_2} \Pi^-_{p_e}(\mathbf{u}) \subseteq \bigcap_{\mathbf{u}\in U_1} \Pi^-_{p_e}(\mathbf{u}).$$

□

C Proof of Proposition 3

The proof will follow from the Voronoi-Delaunay duality, which tells us that the Voronoi cells are convex polytopes with vertices corresponding to circumcenters of the Delaunay simplices. In particular, the vertices of $\mathrm{Vor}(\mathbf{o}, \mathcal{S}^{\mathbf{o}}_{p_e}(U))$ are the circumcenters of the simplices in $\{\tau \in \mathcal{D} \mid \mathbf{o} \in \tau\}$, where $\mathcal{D}$ is any Delaunay triangulation of the point set $\{\mathbf{o}\} \cup S^{\mathbf{o}}_{p_e}(U)$.

Assume that $\mathcal{D}$ is such a Delaunay triangulation, and that there exists a point $\mathbf{s}^* \in \mathcal{S}^{\mathbf{o}}_{p_e}(U)$ such that $\mathbf{s}^*$ and $\mathbf{o}$ are not connected by $\mathcal{D}$. This means (by definition) that any simplex in $\mathcal{D}$ containing $\mathbf{o}$ does not contain $\mathbf{s}^*$, and vice versa. Hence,

$$\mathrm{Vor}(\mathbf{o}, \mathcal{S}^{\mathbf{o}}_{p_e}(U)) = \mathrm{Vor}(\mathbf{o}, \mathcal{S}^{\mathbf{o}}_{p_e}(U) \setminus \{\mathbf{s}^*\}).$$

We now let $\mathbf{u}^* \in U$ denote the unit vector corresponding to $\mathbf{s}^*$, i.e. $\mathbf{s}^* = \mathbf{s}^{\mathbf{o},\mathbf{u}^*}_{p_e}$. Making use of Lemma 1 we then observe that

$$\mathrm{Vor}(\mathbf{o}, \mathcal{S}^{\mathbf{o}}_{p_e}(U)) = \mathrm{Vor}(\mathbf{o}, \mathcal{S}^{\mathbf{o}}_{p_e}(U) \setminus \{\mathbf{s}^*\}) \Rightarrow \bigcap_{\mathbf{u}\in U} \Pi^-_{p_e}(\mathbf{u}) = \bigcap_{\mathbf{u}\in U\setminus\{\mathbf{u}^*\}} \Pi^-_{p_e}(\mathbf{u}). \tag{12}$$

This means that, either 1) $\Pi_{p_e}(\mathbf{u}^*) \cap \mathrm{Vor}(\mathbf{o}, \mathcal{S}^{\mathbf{o}}_{p_e}(U)) = \emptyset$, or 2) that there exists some vertex $\mathbf{v}^*$ of $\mathrm{Vor}(\mathbf{o}, \mathcal{S}^{\mathbf{o}}_{p_e}(U))$ such that $\mathbf{v}^* \in \Pi_{p_e}(\mathbf{u}^*) \cap \mathrm{Vor}(\mathbf{o}, \mathcal{S}^{\mathbf{o}}_{p_e}(U))$. From Proposition 2 we have that $\mathcal{B}_{p_e} \subseteq \mathrm{Vor}(\mathbf{o}, \mathcal{S}^{\mathbf{o}}_{p_e}(U))$. Since we assume that $\partial\mathcal{B}_{p_e}$ is a proper convex environmental contour, $\Pi_{p_e}(\mathbf{u}^*) \cap \mathcal{B}_{p_e} \neq \emptyset$, and so

$$\Pi_{p_e}(\mathbf{u}^*) \cap \mathrm{Vor}(\mathbf{o}, \mathcal{S}^{\mathbf{o}}_{p_e}(U)) \neq \emptyset. \tag{13}$$

From (12) and (13) we can therefore conclude that there exists some vertex $\mathbf{v}^*$ of $\mathrm{Vor}(\mathbf{o}, \mathcal{S}^{\mathbf{o}}_{p_e}(U))$ such that $\mathbf{v}^* \in \Pi_{p_e}(\mathbf{u}^*) \cap \mathrm{Vor}(\mathbf{o}, \mathcal{S}^{\mathbf{o}}_{p_e}(U))$.

We then observe that

$$\mathbf{v}^* \in \Pi_{p_e}(\mathbf{u}^*) \Rightarrow \|\mathbf{v}^* - \mathbf{o}\| = \|\mathbf{s}^* - \mathbf{o}\|. \tag{14}$$

This follows from the definition of $\Pi_{p_e}(\cdot)$ and the set $S^{\mathbf{o}}_{p_e}(U)$, which says that $\mathbf{s}^*$ is the reflection of $\mathbf{o}$ with respect to the hyperplane $\Pi_{p_e}(\mathbf{u}^*)$. Now, since $\mathbf{v}^*$ is also a vertex of $\mathrm{Vor}(\mathbf{o}, \mathcal{S}^{\mathbf{o}}_{p_e}(U))$, then

$\mathbf{v}^*$ is the circumcenter of a Delaunay simplex τ, with $\mathbf{o} \in \tau$. From (14) we see that $\mathbf{s}^*$ also lies on this circum-hypersphere, together with $\mathbf{o}$. Hence, if the Delaunay triangulation $\mathcal{D}$ was unique, we could conclude that $\{\mathbf{s}^*, \mathbf{o}\} \subset \tau \in \mathcal{D}$, which contradicts the initial assumption that $\mathbf{s}^*$ and $\mathbf{o}$ are not connected in $\mathcal{D}$.

In the case where there is no *unique* Delaunay triangulation of the point set $\{\mathbf{o}\} \cup S^{\mathbf{o}}_{p_e}(U)$, the fact that $\mathbf{s}^*$ and $\mathbf{o}$ lie on the same circum-hypersphere of *some* Delaunay simplex τ lets us conclude that there exists *some* Delaunay triangulation $\mathcal{D}'$ where $\mathbf{s}^*$ and $\mathbf{o}$ are part of the same simplex. We can therefore conclude that, if there exists a Delaunay triangulation $\mathcal{D}$ that does not connect $\mathbf{s}^*$ and $\mathbf{o}$, then there must exist a different Delaunay triangulation $\mathcal{D}'$ that connects $\mathbf{s}^*$ and $\mathbf{o}$.

□

D Proof of Proposition 4

For any $\mathbf{u} \in \mathcal{U}$ we first recall that the existence of some $\mathbf{b} \in \Pi_{p_e}(\mathbf{u}) \cap \partial\mathcal{B}_{p_e}$ follows from the definition of proper convex environmental contours. We then note that, as any element of $\mathcal{S}^{\mathbf{o}}_{p_e}(\mathcal{U})$ is of the form $\mathbf{s}^{\mathbf{o},\mathbf{u}}_{p_e} = \mathbf{o} + 2C^{\mathbf{o}}_{p_e}(\mathbf{u})\mathbf{u}$, we have that

$$\begin{aligned}\left\|\mathbf{s}^{\mathbf{o},\mathbf{u}}_{p_e} - \mathbf{b}\right\|^2 &= \left\|\mathbf{o} - \mathbf{b} + 2C^{\mathbf{o}}_{p_e}(\mathbf{u})\mathbf{u}\right\|^2 = \|\mathbf{o} - \mathbf{b}\|^2 + 4(C^{\mathbf{o}}_{p_e}(\mathbf{u}))^2 + 4C^{\mathbf{o}}_{p_e}(\mathbf{u})(\mathbf{o} - \mathbf{b}) \cdot \mathbf{u}. \\ &= \|\mathbf{o} - \mathbf{b}\|^2 + 4C^{\mathbf{o}}_{p_e}(\mathbf{u}) \left(C^{\mathbf{o}}_{p_e}(\mathbf{u}) - (\mathbf{b} - \mathbf{o}) \cdot \mathbf{u}\right).\end{aligned} \tag{15}$$

Now if $\mathbf{b} \in \Pi_{p_e}(\mathbf{u})$ we have that $(\mathbf{b} - \mathbf{o}) \cdot \mathbf{u} = C^{\mathbf{o}}_{p_e}(\mathbf{u})$ (by definition), and hence $\left\|\mathbf{s}^{\mathbf{o},\mathbf{u}}_{p_e} - \mathbf{b}\right\|^2 = \|\mathbf{o} - \mathbf{b}\|^2$, which means that $\mathbf{s}^{\mathbf{o},\mathbf{u}}_{p_e} \in \partial\mathcal{W}^{\mathbf{o}}(\mathbf{b})$.

The statement that $\mathcal{S}^{\mathbf{o}}_{p_e}(\mathcal{U}) \cap \mathcal{W}^{\mathbf{o}}(\mathbf{b}) \subseteq \partial\mathcal{W}^{\mathbf{o}}(\mathbf{b})$ means that there are no $\mathbf{u}' \in \mathcal{U}$ such that $\mathbf{s}^{\mathbf{o},\mathbf{u}'}_{p_e}$ lies in the interior of the ball $\mathcal{W}^{\mathbf{o}}(\mathbf{b})$. Assume, on the contrary, that there exists some $\mathbf{s}^{\mathbf{o},\mathbf{u}'}_{p_e} \in \mathcal{W}^{\mathbf{o}}(\mathbf{b}) \setminus \partial\mathcal{W}^{\mathbf{o}}(\mathbf{b})$. Then $\left\|\mathbf{s}^{\mathbf{o},\mathbf{u}'}_{p_e} - \mathbf{b}\right\| < \|\mathbf{o} - \mathbf{b}\|$ by definition. From (15) we then have that $4C^{\mathbf{o}}_{p_e}(\mathbf{u}') \left(C^{\mathbf{o}}_{p_e}(\mathbf{u}') - (\mathbf{b} - \mathbf{o}) \cdot \mathbf{u}'\right) < 0$. We have assumed that $\mathbf{o} \in \mathcal{B}_{p_e} \setminus \partial\mathcal{B}_{p_e}$, and so by Lemma 1 $C^{\mathbf{o}}_{p_e}(\mathbf{u}') > 0$. Hence,

$$\mathbf{s}^{\mathbf{o},\mathbf{u}'}_{p_e} \in \mathcal{W}^{\mathbf{o}}(\mathbf{b}) \setminus \partial\mathcal{W}^{\mathbf{o}}(\mathbf{b}) \Rightarrow C^{\mathbf{o}}_{p_e}(\mathbf{u}') - (\mathbf{b} - \mathbf{o}) \cdot \mathbf{u}' < 0.$$

But this means that $\mathbf{b} \in \Pi^+_{p_e}(\mathbf{u}')$, which is impossible when $\mathbf{b} \in \partial\mathcal{B}_{p_e}$.

□

E Proof of Lemma 2

We first observe that the condition 1) is just a different way of stating that a point is on the hyperplane $\Pi_{p_e}(\mathbf{u})$ (alternatively, compute the norms as in (15) and note that $C^{\mathbf{o}}_{p_e}(\mathbf{u}) > 0$). That is, for any $\mathbf{x} \in \mathbb{R}^n$, we have $\mathbf{x} \in \Pi_{p_e}(\mathbf{u}) \Leftrightarrow \|\mathbf{x} - \mathbf{o}\| = \left\|\mathbf{s}^{\mathbf{o},\mathbf{u}}_{p_e} - \mathbf{x}\right\|$.

Hence, $\mathbf{a} \in \Pi_{p_e}(\mathbf{u})$ by condition 1). Then, by Proposition 4 there exists some $\mathbf{b} \in \Pi_{p_e}(\mathbf{u}) \cap \partial\mathcal{B}_{p_e}$ where $\mathcal{S}^{\mathbf{o}}_{p_e}(\mathcal{U}) \cap \mathcal{W}^{\mathbf{o}}(\mathbf{b}) \subseteq \partial\mathcal{W}^{\mathbf{o}}(\mathbf{b})$, and $\mathbf{s}^{\mathbf{o},\mathbf{u}}_{p_e} \in \partial\mathcal{W}^{\mathbf{o}}(\mathbf{b})$. This means that the n-dimensional closed ball $\mathcal{W}^{\mathbf{o}}(\mathbf{b})$, centered at $\mathbf{b}$ with radius $\|\mathbf{b} - \mathbf{o}\|$ is tangent to $\mathcal{S}^{\mathbf{o}}_{p_e}(\mathcal{U})$ at the point $\mathbf{s}^{\mathbf{o},\mathbf{u}}_{p_e}$. As both $\mathcal{S}^{\mathbf{o}}_{p_e}(\mathcal{U})$ and $\mathcal{W}^{\mathbf{o}}(\mathbf{b})$ are differentiable $(n-1)$-dimensional manifolds, they share the same $(n-1)$-dimensional tangent space at $\mathbf{s}^{\mathbf{o},\mathbf{u}}_{p_e}$. We let $V = \{\mathbf{v}_1, \ldots, \mathbf{v}_{n-1}\} \subset \mathbb{R}^n$ denote a basis for this tangent space.

From the above argument, it is clear that also $\mathbf{b}$ satisfies both of the criteria in the Lemma, as 1) $\mathbf{b} \in \Pi_{p_e}(\mathbf{u})$ and 2) $(\mathbf{s}^{\mathbf{o},\mathbf{u}}_{p_e} - \mathbf{b})$ is orthogonal to $\mathcal{S}^{\mathbf{o}}_{p_e}(\mathcal{U})$ at $\mathbf{s}^{\mathbf{o},\mathbf{u}}_{p_e}$ since $(\mathbf{s}^{\mathbf{o},\mathbf{u}}_{p_e} - \mathbf{b})$ is orthogonal to $\mathcal{W}^{\mathbf{o}}(\mathbf{b})$ at $\mathbf{s}^{\mathbf{o},\mathbf{u}}_{p_e}$.

Hence, starting with a pair $(\mathbf{a}, \mathbf{u})$ that satisfies the two conditions of the Lemma, we have identified a point $\mathbf{b} \in \Pi_{p_e}(\mathbf{u}) \cap \partial\mathcal{B}_{p_e}$ such that $(\mathbf{b}, \mathbf{u})$ satisfies the same conditions. Using that $(\mathbf{a}, \mathbf{u})$ and $(\mathbf{b}, \mathbf{u})$ satisfy these conditions simultaneously, we obtain

1. $\Rightarrow \mathbf{a}, \mathbf{b} \in \Pi_{p_e}(\mathbf{u}) \Rightarrow \mathbf{a} \cdot \mathbf{u} = \mathbf{b} \cdot \mathbf{u}$,
2. $\Rightarrow (\mathbf{s}^{\mathbf{o},\mathbf{u}}_{p_e} - \mathbf{a}) \cdot \mathbf{v} = (\mathbf{s}^{\mathbf{o},\mathbf{u}}_{p_e} - \mathbf{b}) \cdot \mathbf{v} = 0$ for any $\mathbf{v} \in V$.

From these conditions we see that $(\mathbf{a}-\mathbf{b})\cdot\mathbf{u}=0$ and $(\mathbf{a}-\mathbf{b})\cdot\mathbf{v}=0$ for any $\mathbf{v}\in V$. Hence, if $\mathbf{u}$ is linearly independent of V, we can conclude that $\mathbf{a}=\mathbf{b}$.

Assume $\mathbf{u}=\sum_{i=1}^{n-1}\alpha_i\mathbf{v}_i$ for some $\alpha_1,\ldots,\alpha_{n-1}\in\mathbb{R}$. Then $(\mathbf{b}-\mathbf{s}_{p_e}^{\mathbf{o},\mathbf{u}})\cdot\mathbf{u}=\sum_{i=1}^{n-1}\alpha_i(\mathbf{b}-\mathbf{s}_{p_e}^{\mathbf{o},\mathbf{u}})\cdot\mathbf{v}_i=0$. Then, by definition of the hyperplane $\mathit{\Pi}_{p_e}(\mathbf{u})$, $C_{p_e}^{\mathbf{o}}(\mathbf{u})=(\mathbf{b}-\mathbf{o})\cdot\mathbf{u}=(\mathbf{b}-\mathbf{s}_{p_e}^{\mathbf{o},\mathbf{u}}+\mathbf{s}_{p_e}^{\mathbf{o},\mathbf{u}}-\mathbf{o})\cdot\mathbf{u}=(\mathbf{s}_{p_e}^{\mathbf{o},\mathbf{u}}-\mathbf{o})\cdot\mathbf{u}$. But this means that $\mathbf{s}_{p_e}^{\mathbf{o},\mathbf{u}}\in\mathit{\Pi}_{p_e}(\mathbf{u})$, which is impossible.

We may therefore conclude that $\mathbf{a}=\mathbf{b}\in\mathit{\Pi}_{p_e}(\mathbf{u})\cap\partial\mathcal{B}_{p_e}$. By the same argument as above, if $\mathbf{b}_1$ and $\mathbf{b}_2$ are two elements of $\mathit{\Pi}_{p_e}(\mathbf{u})\cap\partial\mathcal{B}_{p_e}$, then since $(\mathbf{b}_1,\mathbf{u})$ and $(\mathbf{b}_2,\mathbf{u})$ both satisfy the conditions of the Lemma, we must have $\mathbf{b}_1=\mathbf{b}_2$. Therefore $\mathit{\Pi}_{p_e}(\mathbf{u})\cap\partial\mathcal{B}_{p_e}$ is a singleton set, and we can conclude that $\{\mathbf{a}\}=\mathit{\Pi}_{p_e}(\mathbf{u})\cap\partial\mathcal{B}_{p_e}$.

□

F Proof of Proposition 5

We first recall that if $\partial\mathcal{B}_{p_e}$ is a proper convex environmental contour, then for any $\mathbf{b}\in\partial\mathcal{B}_{p_e}$ there exists some $\mathbf{u}\in\mathcal{U}$ such that $\mathbf{b}\in\mathit{\Pi}_{p_e}(\mathbf{u})$, and so $\partial\mathcal{B}_{p_e}\subset\cup_{\mathbf{u}\in\mathcal{U}}\mathit{\Pi}_{p_e}(\mathbf{u})$.

Then, if $F:\mathcal{U}\to\mathbb{R}^n$ is a mapping such that the assumptions and conditions of Lemma 2 hold for any pair $(F(\mathbf{u}),\mathbf{u})$, Lemma 2 lets us conclude that $\{F(\mathbf{u})\}=\mathit{\Pi}_{p_e}(\mathbf{u})\cap\partial\mathcal{B}_{p_e}$ for any $\mathbf{u}\in\mathcal{U}$.

Hence, $F(\mathcal{U})=\cup_{\mathbf{u}\in\mathcal{U}}(\mathit{\Pi}_{p_e}(\mathbf{u})\cap\partial\mathcal{B}_{p_e})=\partial\mathcal{B}_{p_e}\cap(\cup_{\mathbf{u}\in\mathcal{U}}\mathit{\Pi}_{p_e}(\mathbf{u}))=\partial\mathcal{B}_{p_e}$.

□

G Proof of Theorem 1

If the p_e-level percentile function $C_{p_e}(\mathbf{u})$ is continuously differentiable on the unit $(n-1)$-sphere, then as $\mathbf{s}_{p_e}^{\mathbf{o},\mathbf{u}}=\mathbf{o}+2(C_{p_e}(\mathbf{u})-\mathbf{u}\cdot\mathbf{o})\mathbf{u}$, the set $\mathcal{S}_{p_e}^{\mathbf{o}}(\mathcal{U})=\{s_{p_e}^{\mathbf{o},\mathbf{u}}|\mathbf{u}\in\mathcal{U}\}$ is a differentiable manifold. Hence, the assumptions of Lemma 2 are satisfied.

We first note that, as a consequence of Lemma 2, any supporting hyperplane intersects $\partial\mathcal{B}_{p_e}$ at a single point, which means that $\mathcal{B}_{p_e}$ is strictly convex. For details we refer to the proof of Lemma 2 in Appendix E, where we observe that $\mathit{\Pi}_{p_e}(\mathbf{u})\cap\partial\mathcal{B}_{p_e}$ is a singleton set for any $\mathbf{u}\in\mathcal{U}$, as the pair $(\mathbf{b},\mathbf{u})$ satisfies the conditions in Lemma 2 for any $\mathbf{b}\in\mathit{\Pi}_{p_e}(\mathbf{u})\cap\partial\mathcal{B}_{p_e}$. (And for any $\mathbf{b}\in\partial\mathcal{B}_{p_e}$ we have $\mathbf{b}\in\mathit{\Pi}_{p_e}(\mathbf{u})$ for some $\mathbf{u}$ as $\partial\mathcal{B}_{p_e}$ is proper).

We will show that the proposed parametrization in the theorem is valid using Lemma 2 and Proposition 5. That is, for any $\mathbf{u}=\mathbf{u}(\boldsymbol{\theta})\in\mathcal{U}$, we must show that

1. $\|\mathbf{b}(\boldsymbol{\theta})-\mathbf{o}\|=\left\|\mathbf{s}_{p_e}^{\mathbf{o},\mathbf{u}(\boldsymbol{\theta})}-\mathbf{b}(\boldsymbol{\theta})\right\|$, and
2. $(\mathbf{s}_{p_e}^{\mathbf{o},\mathbf{u}(\boldsymbol{\theta})}-\mathbf{b}(\boldsymbol{\theta}))$ is orthogonal to $\mathcal{S}_{p_e}^{\mathbf{o}}(\mathcal{U})$ at $\mathbf{s}_{p_e}^{\mathbf{o},\mathbf{u}(\boldsymbol{\theta})}$,

for $\mathbf{o}\in\mathcal{B}_{p_e}\setminus\partial\mathcal{B}_{p_e}$. To simplify the notation we will suppress writing out the dependency on $\boldsymbol{\theta}$, and write

$$\mathbf{b}=C_{p_e}\mathbf{u}+\nabla\mathbf{u}\eta^{-1}(\nabla C_{p_e})^T.$$

Using (8) we can express $\mathbf{b}$ in terms of $C_{p_e}^{\mathbf{o}}$:

$$\begin{aligned}\mathbf{b}&=C_{p_e}\mathbf{u}+\nabla\mathbf{u}\eta^{-1}(\nabla C_{p_e})^T\\&=C_{p_e}\mathbf{u}+\mathbf{u}\mathbf{u}^T\mathbf{o}+\nabla\mathbf{u}\eta^{-1}(\nabla C_{p_e}^{\mathbf{o}})^T+\nabla\mathbf{u}\eta^{-1}(\nabla\mathbf{u})^T\mathbf{o}\\&=\mathbf{o}+C_{p_e}^{\mathbf{o}}\mathbf{u}+\nabla\mathbf{u}\eta^{-1}(\nabla C_{p_e}^{\mathbf{o}})^T,\end{aligned}$$

where we made use of the property that $\mathbf{u}\mathbf{u}^T+\nabla\mathbf{u}\eta^{-1}(\nabla\mathbf{u})^T=I$ (i.e. the identity operator). Note that the metric tensor $\eta=(\nabla\mathbf{u})^T\nabla\mathbf{u}$ is invertible because we have assumed a regular parametrization (and so $\nabla\mathbf{u}$ has full rank). To show condition (1) above, we can just compute the norms

$$\begin{aligned}&\|\mathbf{b}-\mathbf{o}\|^2-\left\|\mathbf{s}_{p_e}^{\mathbf{o},\mathbf{u}}-\mathbf{b}\right\|^2\\&=\left\|C_{p_e}^{\mathbf{o}}\mathbf{u}+\nabla\mathbf{u}\eta^{-1}(\nabla C_{p_e}^{\mathbf{o}})^T\right\|^2-\left\|C_{p_e}^{\mathbf{o}}\mathbf{u}-\nabla\mathbf{u}\eta^{-1}(\nabla C_{p_e}^{\mathbf{o}})^T\right\|^2\\&=4C_{p_e}^{\mathbf{o}}\mathbf{u}\cdot\nabla\mathbf{u}\eta^{-1}(\nabla C_{p_e}^{\mathbf{o}})^T\\&=0.\end{aligned}$$

Here we have used the fact that $\mathbf{u}\cdot\nabla\mathbf{u}=\mathbf{u}^T\nabla\mathbf{u}=\frac{1}{2}\nabla(\mathbf{u}^T\mathbf{u})=\nabla(1)=0$.

To show condition (2) we will use that the columns of $\nabla \mathbf{s}_{p_e}^{\mathbf{o},\mathbf{u}}$ form a basis of the tangent space of $\mathcal{S}_{p_e}^{\mathbf{o}}(\mathcal{U})$ at $\mathbf{s}_{p_e}^{\mathbf{o},\mathbf{u}}$. The orthogonality condition (2) is therefore equivalent to saying that $\nabla(s_{p_e}^{\mathbf{o},\mathbf{u}})^T(s_{p_e}^{\mathbf{o},\mathbf{u}} - \mathbf{b}) = \mathbf{0}$. But this follows from the definition of $s_{p_e}^{\mathbf{o},\mathbf{u}}$, as $\nabla \mathbf{s}_{p_e}^{\mathbf{o},\mathbf{u}} = \nabla(\mathbf{o} + 2C_{p_e}^{\mathbf{o}}\mathbf{u}) = 2(C_{p_e}^{\mathbf{o}}\nabla\mathbf{u} + \mathbf{u}\nabla C_{p_e}^{\mathbf{o}})$, and hence

$$\begin{aligned}
\frac{1}{2}\nabla(s_{p_e}^{\mathbf{o},\mathbf{u}})^T(s_{p_e}^{\mathbf{o},\mathbf{u}} - \mathbf{b}) &= \left(C_{p_e}^{\mathbf{o}}\nabla\mathbf{u}^T + (\nabla C_{p_e}^{\mathbf{o}})^T\mathbf{u}^T\right)\left(C_{p_e}^{\mathbf{o}}\mathbf{u} - \nabla\mathbf{u}\eta^{-1}(\nabla C_{p_e}^{\mathbf{o}})^T\right) \\
&= (C_{p_e}^{\mathbf{o}})^2\underbrace{\nabla\mathbf{u}^T\mathbf{u}}_{\mathbf{0}} - C_{p_e}^{\mathbf{o}}\underbrace{\nabla\mathbf{u}^T\nabla\mathbf{u}\eta^{-1}}_{I}(\nabla C_{p_e}^{\mathbf{o}})^T \\
&+ C_{p_e}^{\mathbf{o}}(\nabla C_{p_e}^{\mathbf{o}})^T\underbrace{\mathbf{u}^T\mathbf{u}}_{1} - (\nabla C_{p_e}^{\mathbf{o}})^T\underbrace{\mathbf{u}^T\nabla\mathbf{u}}_{\mathbf{0}}\eta^{-1}(\nabla C_{p_e}^{\mathbf{o}})^T \\
&= -C_{p_e}^{\mathbf{o}}(\nabla C_{p_e}^{\mathbf{o}})^T + C_{p_e}^{\mathbf{o}}(\nabla C_{p_e}^{\mathbf{o}})^T \\
&= \mathbf{0}.
\end{aligned}$$

Using Proposition 5 we may then conclude that, given an atlas $\{\mathbf{u}_i(\boldsymbol{\theta}) \mid \boldsymbol{\theta} \in \Theta_i\}_i$ on $\mathcal{U}$ where each $(\mathbf{u}_i, \Theta_i)$ is a regular parametrization, the corresponding charts $(\mathbf{b}_i, \Theta_i)$ is an atlas on $\partial\mathcal{B}_{p_e}$. Finally, differentiability of $\partial\mathcal{B}_{p_e}$ then follows from the given expression for $\mathbf{b}_i$ as a function of $\boldsymbol{\theta}$.

□

H Proof of Lemma 3

We first observe that, as a direct consequence of Definition 1, $\mathbf{X}$ admits a proper convex environmental contour if and only if every hyperplane $\Pi_{p_e}(\mathbf{u})$ is a supporting hyperplane of $\mathcal{B}_{p_e}$. That is, if and only if $\mathcal{B}_{p_e} \cap \Pi_{p_e}(\mathbf{u}) \neq \emptyset$ for all $\mathbf{u} \in \mathcal{U}$.

Hence, if $\mathbf{X}$ admits a proper convex environmental contour, we can select $\mathbf{o} \in \Pi_{p_e}(\mathbf{u}') \cap \partial\mathcal{B}_{p_e}$ which (by Lemma 1) satisfies the condition.

If $\mathbf{X}$ does not admit a proper convex environmental contour, then there is some hyperplane $\Pi_{p_e}(\mathbf{u}')$ that does not intersect B_{p_e}. Hence, for any $\mathbf{o} \in \Pi_{p_e}(\mathbf{u}')$ we have $\mathbf{o} \notin B_{p_e}$, and by Lemma 1 there must exist some $\mathbf{u}^*$ with $C_{p_e}^{\mathbf{o}}(\mathbf{u}^*) < 0$.

□

I Proof of Lemma 4

Dropping the dependency on $\boldsymbol{\theta}$ and p_e for simpler notation, we may write

$$\mathbf{u}^T\mathbf{b} = \mathbf{u}^T(C\mathbf{u} + \nabla\mathbf{u}\eta^{-1}\nabla C^T) = C\mathbf{u}^T\mathbf{u} + \mathbf{u}^T\nabla\mathbf{u}\eta^{-1}\nabla C^T = C,$$

as $\mathbf{u}^T\mathbf{u} = 1$ and $\mathbf{u}^T\nabla\mathbf{u} = \frac{1}{2}\nabla(\mathbf{u}^T\mathbf{u}) = \nabla(1) = 0$. This means that $\mathbf{b}(\boldsymbol{\theta}) \in \Pi(\boldsymbol{\theta})$. Similarly, we observe that

$$\nabla\mathbf{u}^T\mathbf{b} = C\nabla\mathbf{u}^T\mathbf{u} + \nabla\mathbf{u}^T\nabla\mathbf{u}\eta^{-1}\nabla C^T = \nabla C^T,$$

as $\nabla\mathbf{u}^T\nabla\mathbf{u} = \eta$ by definition. From the chain rule we then get $\mathbf{u}^T\nabla\mathbf{b} = \nabla(\mathbf{u}^T\mathbf{b}) - (\nabla\mathbf{u}^T\mathbf{b})^T = \nabla C - \nabla C = \mathbf{0}$. Since the hyperplane $\Pi(\boldsymbol{\theta})$ has normal vector $\mathbf{u}(\boldsymbol{\theta})$, we can conclude that $\Pi(\boldsymbol{\theta})$ is tangential to $\mathbf{b}(\Theta)$ at $\mathbf{b}(\boldsymbol{\theta})$.

□

J Proof of Theorem 2

To simplify notation, we drop the dependency p_e and the index i of the parametrization.

Assume (2) is true and let $\mathcal{B}$ denote the closed convex set. Then Lemma 4 implies that all hyperplanes $\Pi(\boldsymbol{\theta})$ are supporting hyperplanes of $\mathcal{B}$, and so $\partial\mathcal{B}$ is a proper convex environmental contour. The fact that (1) $\Rightarrow$ (2) comes as a direct consequence of Theorem 1, so we have that (1) $\Leftrightarrow$ (2).

To show that (1) $\Rightarrow$ (3), we first note that when $\mathbf{X}$ admits a proper convex environmental contour, then since $\boldsymbol{b}(\boldsymbol{\theta}) \in \Pi(\boldsymbol{\theta})$ (see Lemma 4) it follows from Lemma 1 that $\kappa(\boldsymbol{\theta}|\boldsymbol{\theta}') \geq 0$ for all $\boldsymbol{\theta}$ and $\boldsymbol{\theta}'$. For the converse, assume that $\mathbf{X}$ does not admit a proper convex environmental contour. Then from Lemma 3 there exists some $\mathbf{u}'$ such that for any $\mathbf{o} \in \Pi(\mathbf{u}')$ we can find some $\mathbf{u}$ where

$C^{\mathbf{o}}(\mathbf{u}) < 0$. In forms of the given parametrization, this means that we can find some $\boldsymbol{\theta}$ and $\boldsymbol{\theta}'$ where $C^{\mathbf{o}}(\boldsymbol{\theta}) < 0$ for any $\mathbf{o} \in \Pi(\boldsymbol{\theta}')$. As $\mathbf{b}(\boldsymbol{\theta}') \in \Pi(\boldsymbol{\theta}')$ we have that $\kappa(\boldsymbol{\theta}|\boldsymbol{\theta}') = C^{\mathbf{b}(\boldsymbol{\theta}')}(\boldsymbol{\theta}) < 0$. Hence (1) $\Leftrightarrow$ (3).

Finally, (3) $\Leftrightarrow$ (4) follows from the fact that $\mathbf{b}(\boldsymbol{\theta}') \in \Pi(\boldsymbol{\theta}')$ which means that $\kappa(\boldsymbol{\theta}'|\boldsymbol{\theta}') = 0$.

□

K Proof of Corollary 2

From statement (4) in Theorem 2, $\kappa(\boldsymbol{\theta}|\boldsymbol{\theta}')$ attains a local minimum at $\boldsymbol{\theta} = \boldsymbol{\theta}'$, which means that the matrix $A(\boldsymbol{\theta}) = \nabla_{\boldsymbol{\theta}}\nabla_{\boldsymbol{\theta}}\kappa(\boldsymbol{\theta}|\boldsymbol{\theta}')|_{\boldsymbol{\theta}=\boldsymbol{\theta}'}$ is positive semi-definite $\forall \boldsymbol{\theta} \in \Theta$. Suppressing the notation $\boldsymbol{\theta}$ and p_e we can write

$$\begin{aligned} A &= \nabla\nabla C - \mathbf{b}^T\nabla\nabla\mathbf{u} \\ &= \nabla\nabla C - \left(C\mathbf{u} + \nabla\mathbf{u}\eta^{-1}\nabla C^T\right)^T \nabla\nabla\mathbf{u} \\ &= \left(\nabla\nabla C - \nabla C\eta^{-1}(\nabla\mathbf{u})^T\nabla\nabla\mathbf{u}\right) - C\mathbf{u}^T\nabla\nabla\mathbf{u}. \end{aligned} \tag{16}$$

The first term of (16) (in brackets) can be recognized as the Hessian operator on a Riemann manifold. This is most easily seen when expressed in index form, i.e.,

$$Hess_{ij}(C) = \frac{\partial^2 C}{\partial\theta_i\partial\theta_j} - \Gamma_{ij}^m \frac{\partial C}{\partial\theta_m},$$

where Γ_{ij}^m are known as a Christoffel symbols, defined as

$$\Gamma_{ij}^m = \sum_{k,l} \left(\eta^{-1}\right)_{ml} \frac{\partial u_k}{\partial\theta_l} \frac{\partial^2 u_k}{\partial\theta_i\partial\theta_j}.$$

The last term in the last line of (16) above can be rewritten in terms of the metric tensor η, i.e., $C\mathbf{u}^T\nabla\nabla\mathbf{u} = C\nabla\left(\mathbf{u}^T\nabla\mathbf{u}\right) - C(\nabla\mathbf{u})^T\nabla\mathbf{u} = -\eta C$, because $\mathbf{u}^T\nabla\mathbf{u} = \mathbf{0}$ and $(\nabla\mathbf{u})^T\nabla\mathbf{u} = \eta$. It therefore follows that

$$A(\boldsymbol{\theta}) = \nabla_{\boldsymbol{\theta}}\nabla_{\boldsymbol{\theta}}\kappa(\boldsymbol{\theta}|\boldsymbol{\theta}')|_{\boldsymbol{\theta}=\boldsymbol{\theta}'} = Hess(C(\boldsymbol{\theta})) + \eta(\boldsymbol{\theta})C(\boldsymbol{\theta}).$$

□

References

1. Armstrong, C., Chin, C., Penesis, I., Drobyshevski, Y.: Sensitivity of vessel response to environmental contours of extreme sea states. In: Proc. 34th International Conference on Ocean, Offshore and Arctic Engineering (OMAE 2015). American Society of Mechanical Engineers (ASME) (2015)
2. Aurenhammer, F.: Voronoi diagrams - a survey of a fundamental geometric data structure. ACM Comput. Surv. **23**(3), 345–405 (1991)
3. Baarholm, G.S., Haver, S.: Application of environmental contour lines - a summary of a number of case studies. In: Proc. International Conference on Floating Structures for Deepwater Operations. ASRANet (2009)
4. Baarholm, G.S., Haver, S., Økland, O.D.: Combining contours of significant wave height and peak period with platform response distributions for predicting design response. Marine Structures **23**, 147–163 (2010)
5. Baarholm, G.S., Moan, T.: Application of contour line method to estimate extreme ship hull loads considering operational restrictions. Journal of Ship Research **45**, 228–240 (2001)
6. Baarholm, G.S., Sverre, H., Larsen, C.M.: Wave sector dependent contour lines. In: Proc. 26th International Conference on Offshore Mechanics and Arctic Engineering (OMAE 2007). American Society of Mechanical Engineers (ASME) (2007)
7. Beranger, B., Padoan, S.A., Sisson, S.A.: Estimation and uncertainty quantification for extreme quantile regions. Extremes **24**, 349–375 (2021)
8. Bitner-Gregersen, E.: Joint long term models of met-ocean parameters. In: C. Guedes Soares (ed.) Marine Technology and Engineering: CENTEC Anniversary Book. CRC Press (2012)
9. Bitner-Gregersen, E., Haver, S.: Joint long term description of environmental parameters for structural response calculation. In: Proc. 2nd International Workshop on Wave Hindcasting and Forecasting (1989)
10. Bitner-Gregersen, E., Haver, S.: Joint environmental model for reliability calculations. In: Proc. 1st International Offshore and Polar Engineering conference (ISOPE 1991). The International Society of Offshore and Polar Engineering (ISOPE) (1991)
11. Bitner-Gregersen, E.M.: Joint met-ocean description for design and operation of marine structures. Applied Ocean Research **51**, 279–292 (2015)
12. Chai, W., Leira, B.J.: Environmental contours based on inverse SORM. Marine Structures **60**, 34–51 (2018)

13. Chebana, F., Ouarda, T.: Multivariate quantiles in hydrological frequency analysis. Environmetrics **22**, 63–78 (2011)
14. Coles, S.: An Introduction to Statistical Modeling of Extreme Values. Springer-Verlag (2001)
15. Coles, S.G., Tawn, J.A.: Statistical methods for multivariate extremes: an application to structural design. Journal of the Royal Statisticsl Society. Series C (Applied Statistics) **43**(1), 1–48 (1994)
16. Cooley, D., Thibaud, E., Castillo, F., Wehner, M.F.: A nonparametric method for producing isolines of bivariate exceedance probabilities. Extremes **22**, 373–390 (2019)
17. Dahl, K.R., Huseby, A.B.: Buffered environmental contours. In: Proc. ESREL 2018. European Safety and Reliability Association(ESRA) (2018)
18. Derbanne, Q., da Hauteclocque, G.: A new approach for environmental contour and multivariate de-clustering. In: Proc. 38th International Conference on Ocean, Offshore and Arctic Engineering (OMAE 2019). American Society of Mechanical Engineers (ASME) (2019)
19. Eckert-Gallup, A.C., Sallaberry, C.J., Dallman, A.R., Neary, V.S.: Application of principal component analysis (PCA) and imrpoved joint probability distributions to the inverse first-order reliability method (I-FORM) for predicting extreme sea states. Ocean Engineering **112**, 307–319 (2016)
20. Einmahl, J.H.J., de Haan, L., Krajina, A.: Estimating extreme bivariate quantile regions. Extremes **16**, 121–145 (2013)
21. l. Epstein, C.: Convex regions, shadows, and the Gauss map. URL `https://www.math.upenn.edu/~cle/papers/slatgm.pdf`
22. Girard, S., Stupfler, G.: Extreme geometric quantiles in a multivariate regular variation framework. Extremes **18**, 629–663 (2015)
23. GL, D.: Environmental Conditions and Environmental Loads. DNV GL (2017). DNVGL-RP-C205
24. Haghayeghi, Z.S., Ketabdari, M.J.: Development of environmental contours for circular and linear metocean variables. International Journal of Renewable Energy Research **7**, 682–693 (2017)
25. Haselsteiner, A.F., Ohlendorf, J.H., Wosniok, W., Thoben, K.D.: Deriving environmental contours from highest density regions. Coastal Engineering **123**, 42–51 (2017)
26. Haver, S.: Analysis of uncertainties related to the stochastic modelling of ocean waves. Tech. Rep. UR-80-09, Norges tekniske høgskole (1980)
27. Haver, S.: On the joint distribution of heights and periods of sea waves. Ocean Engineering **14**, 359–376 (1987)
28. Haver, S., Bruserud, K.: Environmental contour method: An approximate method for obtaining characteristic response extremes for design purposes. In: Proc. 13th International Workshop on Wave Hindcasting and Forecasting & 4th Coastal Hazard Symposium (2013)
29. Haver, S., Winterstein, S.: Environmental contour lines: A method for estimating long term extremes by a short term analysis. Transactions of the Society of Naval Architects and Marine Engineers **116**, 116–127 (2009)
30. Heffernan, J.E., Tawn, J.A.: A conditional approach for multivariate extreme values. Journal of the Royal Statistical Society Series B **66**, 497–546 (2004)
31. Horn, J.T., Bitner-Gregersen, E., Krokstad, J., Leira, B.J., Amdahl, J.: A new combination of conditional environmental distributions. Applied Ocean Research **73**, 17–26 (2018)
32. Huseby, A.B., Vanem, E., Agrell, C., Hafver, A.: Convex environmental contours. Ocean Engineering **235**, 109366 (2021)
33. Huseby, A.B., Vanem, E., Barbosa, M.H.: Environmental contours for mixtures of distributions. In: Proc. ESREL 2019, pp. 839–846. European Safety and Reliability Association(ESRA) (2019)
34. Huseby, A.B., Vanem, E., Eskeland, K.: Evaluating properties of environmental contours. In: Proc. ESREL 2017. European Safety and Reliability Association(ESRA) (2017)
35. Huseby, A.B., Vanem, E., Natvig, B.: A new approach to environmental contours for ocean engineering applications based on direct Monte Carlo simulations. Ocean Engineering **60**, 124–135 (2013)
36. Huseby, A.B., Vanem, E., Natvig, B.: A new Monte Carlo method for environmental contour estimation. In: Proc. ESREL 2014. European Safety and Reliability Association(ESRA) (2014)
37. Huseby, A.B., Vanem, E., Natvig, B.: Alternative environmental contours for structural reliability analysis. Structural Safety **54**, 32–45 (2015)
38. Jonathan, P., Ewans, K.: Statistical modelling of extreme ocean environments for marine design: a review. Ocean Engineering **62**, 91–109 (2013)
39. Jonathan, P., Ewans, K., Flynn, J.: On the estimation of ocean engineering design contours. In: Proc. 30th International Conference on Ocean, Offshore and Arctic Engineering (OMAE 2011). American Society of Mechanical Engineers (ASME) (2011)
40. Juri, A., Wüthrich, M.V.: Tail dependence from a distributional point of view. Extremes **6**, 213–246 (2004)
41. Leira, B.J.: A comparison of stochastic process models for definition of design contours. Structural Safety **30**, 493–505 (2008)
42. Leonard, I., Lewis, J.: Geometry of Convex Sets. Wiley (2015)
43. Li, Q., Gao, Z., Moan, T.: Modified environmental contour method for predicting long-term extreme responses of bottom-fixed offshore wind turbines. Marine Structures **48**, 15–32 (2016)
44. van de Lindt, J., Niedzwecki, J.: Environmental contour analysis in earthquake engineering. Engineering Structures **22**, 1661–1676 (2000)
45. Lutes, L.D., Winterstein, S.R.: A dynamic inverse FORM method: Design contours for load combination problems. Probabilistic Engineering Mechanics **44**, 118–127 (2016)
46. M. Schaller, F., Kapfer, S., Evans, M., J.F. Hoffmann, M., Aste, T., Saadatfar, M., Mecke, K., W. Delaney, G., Schröder-Turk, G.: Set Voronoi diagrams of 3D assemblies of aspherical particles. Philosophical Magazine **93** (2013)
47. Mackay, E., Haselsteiner, A.f.: Marginal and total exceedance probabilities of environmental contours. Marine Structures **75**, 102863 (2021)
48. Manuel, L., Nguyen, P.T., Canning, J., Coe, R.G., Eckert-Gallup, A.C., Martin, N.: Alternative approaches to develop environmental contours from metocean data. Journal of Ocean Engineering and Marine Energy **4**, 293–310 (2018)
49. Marsaglia, G.: Choosing a point from the surface of a sphere. Ann. Math. Statist. **43**(2), 645–646 (1972)

50. Martini, H., Montejano, L., Oliveros, D.: Bodies of constant width. Springer (2019)
51. Montes-Iturrizaga, R., Heredia-Zavoni, E.: Environmental contours using copulas. Applied Ocean Research **52**, 125–139 (2015)
52. Montes-Iturrizaga, R., Heredia-Zavoni, E.: Multivariate environmental contours using C-vine copulas. Ocean Engineering **118**, 68–82 (2016)
53. Montes-Iturrizaga, R., Heredia-Zavoni, E.: Assessment of uncertainty in environmental contours due to parametric uncertainty in models of the dependence structure between metocean variables. Applied Ocean Research **64**, 86–104 (2017)
54. Muliawan, M.J., Gao, Z., Moan, T.: Application of the contour line method for estimating extreme responses in the mooring lines of a two-body floating wave energy converter. Journal of Offshore Mechanics and Arctic Engineering **135**, 031301:1–10 (2013)
55. Nerzic, R., Frelin, C., Prevesto, M., Quiniou-Ramus, V.: Joint distribution of wind/waves/current in West Africa and derivation of multivariate extreme I-FORM contours. In: Proc. 17th International Offshore and Polar Engineering Conference (ISOPE 2007). The International Society of Offshore and Polar Engineering (ISOPE) (2007)
56. Niedzwwecki, J.M., van de Lindt, J., Yao, J.: Estimating extreme tendon response using environmental contours. Engineering Structures **20**, 601–607 (1998)
57. NORSOK: NORSOK Standard N-003:2017. Action and action effects (2017). Edition 3
58. Okabe, A., Boots, B., Sugihara, K., Chiu, S.N.: Spatial Tessellations: Concepts and Applications of Voronoi Diagrams, 2nd ed. edn. Series in Probability and Statistics. John Wiley and Sons, Inc. (2000)
59. Orsero, P., Fontaine, E., Quiniou, V.: Reliability and response based design of a moored FPSO in West Africa using multivariate environmental contours and response surfaces. In: Proc. 17th International Offshore and Polar Engineering Conference (ISOPE 2007). The International Society of Offshore and Polar Engineering (ISOPE) (2007)
60. Raillard, N., Prevesto, M., Pineau, H.: 3-d environmental extreme value models for the tension in a mooring line of a semi-submersible. Ocean Engineering **184**, 23–31 (2019)
61. Rootzén, H., Segers, J., Wadsworth, J.L.: Multivariate peaks over threshold models. Extremes **21**, 115–145 (2018)
62. Ross, E., Astrup, O.C., Bitner-Gregersen, E., Bunn, N., Feld, G., Gouldby, B., Huseby, A., Liu, Y., Randell, D., Vanem, E., Jonathan, P.: On environmental contours for marine and coastal design. Ocean Engineering **195**, 106194 (2019)
63. Saranyasoontorn, K., Manuel, L.: Efficient models for wind turbine extreme loads using inverse reliability. Journal of Wind Engineering and Industrial Aerodynamics **92**, 789–804 (2004)
64. Saranyasoontorn, K., Manuel, L.: Design loads for wind turbines using the environmental contour method. In: 44th AIAA Aerospace Sciences Meeting and Exhibit, pp. AIAA 2006–1365. American Institute of Aeronautics and Astronautics (AIAA) (2006)
65. Serinaldi, F.: Dismissing return periods! Stochastic Environmental Research and Risk Assessment **29**, 1179–1189 (2015)
66. Shephard, G.C.: Shadow systems of convex sets. Israel Journal of Mathematics **2**(4), 229–236 (1964)
67. Shooter, R., Tawn, J., Ross, E., Jonathan, P.: Basin-wide spatial conditional extremes for severe ocean storms. Extremes **24**, 241–265 (2021)
68. Silva-González, F., Heredia-Zavoni, E., Montes-Iturrizaga, R.: Development of environmental contours using Nataf distribution model. Ocean Engineering **58**, 27–34 (2013)
69. Vanem, E.: Joint statistical models for significant wave height and wave period in a changing climate. Marine Structures **49**, 180–205 (2016)
70. Vanem, E.: A comparison study on the estimation of extreme structural response from different environmental contour methods. Marine Structures **56**, 137–162 (2017)
71. Vanem, E.: 3-dimensional environmental contours based on a direct sampling method for structural reliability analysis of ships and offshore structures. Ships and Offshore Structures **14**, 74–85 (2018)
72. Vanem, E.: A simple approach to account for seasonality in the description of extreme ocean environments. Marine Systems & Ocean Technology **13**, 63–73 (2018)
73. Vanem, E.: Environmental contours for describing extreme ocean wave conditions based on combined datasets. Stochastic Environmental Research and Risk Assessment **33**, 957–971 (2019)
74. Vanem, E.: Bivariate regional extreme value analysis for significant wave height and wave period. Applied Ocean Research **101**, 102266:1–15 (2020)
75. Vanem, E., Bitner-Gregersen, E.M.: Alternative environmental contours for marine structural design - a comparison study. Journal of Offshore Mechanics and Arctic Engineering **137**, 051601:1–8 (2015)
76. Vanem, E., Brandsæter, A.: Unsupervised anomaly detection based on clustering methods and sensor data on a marine diesel engine. Journal of Marine Engineering & Technology **Latest Articles** (2019)
77. Vanem, E., Gramstad, O., Bitner-Gregersen, E.M.: A simulation study on the uncertainty of environmental contours due to sampling variability for different estimation methods. Applied Ocean Research **91**, 101870 (2019)
78. Vanem, E., Guo, B., Ross, E., Jonathan, P.: Comparing different contour methods with response-based methods for extreme ship response analysis. Marine Structures **69**, 102680 (2919)
79. de Waal, D., van Gelder, P.: Modelling of extreme wave heights and periods through copulas. Extremes **8**, 345–356 (2005)
80. Winterstein, S., Ude, T., Cornell, C., Bjerager, P., Haver, S.: Environmental parameters for extreme response: Inverse FORM with omission factors. In: Proc. 6th International Conference on Structural Safety and Reliability (1993)
81. Winterstein, S.R., Jha, A.K., Kumar, S.: Reliability of floating structures: Extreme response and load factor design. Journal of Waterway, Port, Coastal and Ocean Engineering **125**, 163–169 (1999)